frontiers in Earth Science

ORIGINAL RESEARCH
published: 04 August 2020
doi: 10.3389/feart.2020.00330

Structural Evolution of Extended Continental Crust Deciphered From the Cretaceous Batholith in SE China, a Kinmen Island Perspective

*Tsung-Han Huang[1] and Meng Wan Yeh[2]**

[1] Department of Geosciences, National Taiwan University, Taipei, Taiwan, [2] Department of Earth Sciences, National Taiwan Normal University, Taipei, Taiwan

The continental crust of southeast Asia underwent from thickening, thinning to almost rifting during the Mesozoic era as the active continental margin transformed into a passive one. Such crustal thinning history is well-preserved in the Kinmen Island, as the lower crustal granitoids retrograded and rapidly exhumed to surface that were crosscutted by mafic dike swarm. Kinmen Island is situated on the SE coast of Asia, featured by the widespread Cretaceous magmatism as the Paleo-Pacific plate subducted and rollbacked underneath the South China block. Although these complex magmatism are well reported and studied, their associated structural evolution and plate kinematics have not been clearly deciphered. Detailed field mapping, structural measurement, and petrographic analysis of the Kinmen Island were conducted. Up to five deformation events accompanied with five relevant magmatic episodes as well as their corresponding kinematic setting are reconstructed. The ∼129 Ma Chenggong Tonalite (G_1) preserved all deformation events identified in this study, which marks the lower bound timing of all reported events. D_1 formed a gneiss dome with the Taiwushan Granite (∼139 Ma) at the core bounded by moderately dipping gneissic foliation (S_1) as crust extended. D_2 formed subhorizontal S-tectonite (S_2) with further exhumation of D_1 gneiss dome due to middle-to-lower crustal flow associated with further crustal thinning. D_3 formed a sinistral ENE-WSW striking steeply S dipping shear belts with well-developed S/C/C' fabrics. The moderately E-plunging lineation on C surface indicates its transtensional nature. Widespread garnet-bearing leucogranite (G_2) associated with decompressional melting showed long lasting intrusion prior to D_2 until post D_3. D_4 was the intrusion of biotite-bearing Tienpu Granite (∼100 Ma; G_3) that truncated G_1, G_2, and all fabrics, which was followed by the intrusion of E-W striking, steeply dipping biotite-bearing pegmatite (G_4) as the crust further extended. The youngest deformation event (D_5) was NE-SW striking subvertical mafic dike swarm (G_5; 90–76 Ma) due to mantle upwelling through significantly thinned crust. By integrating the structural evolution and the previously reported strain pattern, we delineate the slab rollback direction of the Paleo-pacific plate, which changed from northeastward (129∼114 Ma) to southeastward (107∼76 Ma). This plate kinematic movement switched during 114–107 Ma.

Keywords: Cretaceous magmatism, structural evolution, Paleo-Pacific plate, extended continental crust, slab rollback

OPEN ACCESS

Edited by:
Kwan-Nang Pang, Academia Sinica, Taiwan

Reviewed by:
Kong-Yang Zhu, Zhejiang University, China
Wei Lin, Chinese Academy of Sciences (CAS), China

****Correspondence:***
Meng Wan Yeh
marywyeh@ntnu.edu.tw

Specialty section:
This article was submitted to Petrology, a section of the journal Frontiers in Earth Science

Received: *28 March 2020*
Accepted: *15 July 2020*
Published: *04 August 2020*

Citation:
Huang T-H and Yeh MW (2020) Structural Evolution of Extended Continental Crust Deciphered From the Cretaceous Batholith in SE China, a Kinmen Island Perspective. Front. Earth Sci. 8:330. doi: 10.3389/feart.2020.00330

INTRODUCTION

The most profound tectono-structural features along the continental margin of southeast Asia are the hundreds-kilometer scale spreading of the Cretaceous magmatism along with the development of hundreds-kilometer long NE-SW trending metamorphic belt (e.g., Pingtan-Dongshan metamorphic belt; PDMB) and shear zone (e.g., Changle-Nanao Shear Zone; CNSZ; **Figure 1**). The geodynamic origin of these widespread Mesozoic tectono-magmatic events and associated metamorphism and structural evolution had aroused large interests and controversies over the past decades (e.g., Li and Li, 2007; Li J. et al., 2014; Dong et al., 2018; Mai et al., 2018; Huang et al., 2019). Numerous tectonic models were proposed for the generation of these magmatic events: (1) subduction and rollback/retreat of the Paleo-Pacific plate beneath the Cathaysia block (e.g., John et al., 1990; Zhou and Li, 2000; Zhou et al., 2006; Li and Li, 2007; Sun et al., 2007; Wong et al., 2009; Wang et al., 2011, 2013; Liu et al., 2012; Li J. et al., 2014; Mao et al., 2014; Yang et al., 2018); (2) collision between the Huanan and Dongnanya continental block (Hsü et al., 1990); (3) mantle plume activities (Xie et al., 2001). Despite the diverse tectonic models, the Cretaceous magmatic events are generally accepted as their association to the crustal thinning during the tectonic interaction between the Paleo-Pacific plate and the Eurasian plate. This Mesozoic tectonic event is extremely influential as it not only shapes the present geological framework of the East Asia from Japan to Vietnam, but also layouts the foundation for the development and evolution of basins along the marginal seas (e.g., Mai et al., 2018).

Based on abundant geochemistry data, the alternated crustal shortening (∼170–136 Ma) followed by extension (∼135–90 Ma) related to subduction, back-arc extension to slab break off and mantle flare up were recognized for the Cretaceous tectono-magmatic events (e.g., Li, 2000; Zhou et al., 2006; Wong et al., 2009; Li Z. et al., 2014; Dong et al., 2018; Yang et al., 2018). Two episodes of A-type granite intrusions were noted: 140–120 Ma mainly in the Zhejiang Province and 100–90 Ma along the coastal region of the Fujian Province (**Figure 1B**; Li, 2000; Yang et al., 2012; Li et al., 2013; Li Z. et al., 2014; Zhao et al., 2018). Based on the temporal and spatial correlation of the Jurassic and Cretaceous magmatic bodies, three general evolution patterns were recognized and proposed. One is that the magmatic activity migrated toward southeast during 180–80 Ma due to the steepening of subduction angle of the Paleo-Pacific plate (e.g., Zhou and Li, 2000). The second is the northeastward younging trend of igneous rocks from 180 to 125 Ma owing to northeastward slab rollback of the southwestward obliquely subducted Pacific plate (e.g., Wang et al., 2011). The third is the west to east younging trend of the igneous rocks from 190 to 100 Ma due to slab rollback and/or break-off of the Paleo-Pacific plate (e.g., Wong et al., 2009). Due to the complexity and inconsistency of previously recognized temporal and spatial patterns, Dong et al. (2018) and Mao et al. (2014) suggested the presence of multi-plate convergence with multidirectional extrusion and extension tectonism should be considered. Although the distribution and geochemistry signatures of magmatic rocks are good proxies to decipher the tectonic setting and crustal evolution, the strain setting and the kinematic evolution would be more clearly revealed via detailed structural pattern mapping along the margin of continental crust. Nonetheless, such studies were absent previously. In this study, we depicted the Kinmen Island (**Figure 2**), which is situated on the SE edge of the Eurasian continental margin, as a window to delineate the structural and plate kinematic evolution since Cretaceous time.

GEOLOGICAL BACKGROUND

The continental lithosphere within the southeast region of the Eurasian plate is comprised of the South China block and the Indochina block. The South China block is composed of the Yangtze Block to the northwest, and the Cathaysia Block to the southeast (**Figure 1A**). The southeast region of the Cathaysia Block is characterized by extensive distribution of Jurassic to Cretaceous plutonics, volcanics, NE-trending sinistral CNSZ, and the PDMB along the coast (**Figure 1**; Wang et al., 2013; Li J. et al., 2014). Three major magmatic periods of: ∼187 Ma, 147–130 Ma, and 125–90 Ma were noted, but the Cretaceous magmatism mostly affected areas along the southeast coast (e.g., Liu et al., 2016 and references within). The Cretaceous geological features resulted from the tectono-magmatic events induced by the subduction and retreat of the Paleo-Pacific plate beneath the South China Block (Liu et al., 2012; Zhang et al., 2012; Wang et al., 2013; Li J. et al., 2014; Li Z. et al., 2014; Li et al., 2015; Mao et al., 2014). These Cretaceous rocks consist of high-K calc-alkaline I-type granites with minor A-type granites and gabbros as well as acidic to basaltic volcanic rocks (Li, 2000; Zhou et al., 2006; Li Z. et al., 2014). Extensional setting associated to their generation were delineated from the intimate temporal-spatial characteristics of the 115–95 Ma gabbro with the surrounding I-type granitoids, and the 100–90 Ma A-type granites in the Fujian Province (Li Z. et al., 2014). The bimodal signatures of the 115–95 Ma gabbro and I-type granitoids (Li Z. et al., 2014), and the 94–81 Ma bimodal volcanism further support such interpretation (Chen et al., 2004). These Cretaceous magmatic rocks were later intruded by NE-trending mafic dykes (Lee, 1994; Zhao et al., 2007).

Similar lithology was also noted from the Kinmen Island offshore the Fujian Province, on the leading edge of the continental margin of the South China Block. Four Cretaceous granitoid bodies were mapped out (**Figure 2A**): the Taiwushan Granite (139 Ma, Yui et al., 1996), the Chenggong Tonalite (129 Ma, Lin et al., 2011), the Doumen Granite (120 Ma, Lin et al., 2011), and the Tienpu Granite (100 Ma, Yui et al., 1996), all of which were intruded by the 90–76 Ma mafic dike swarms (Lee, 1994; Lan et al., 1995; Lin et al., 2011). These Cretaceous granitoids were inferred to evolve from the same parental magma under separate stages of fractional crystallization from post-orogenic to continental extension (Lan et al., 1997). The later mafic dike swarms intruded along the NE-trending fractures (Lee, 1994; Lin, 1994; Lan et al., 1997; Lin et al., 2011). The intrusion depth of the Taiwushan Granite was considered to be 28–30 km according to the Al-hornblende

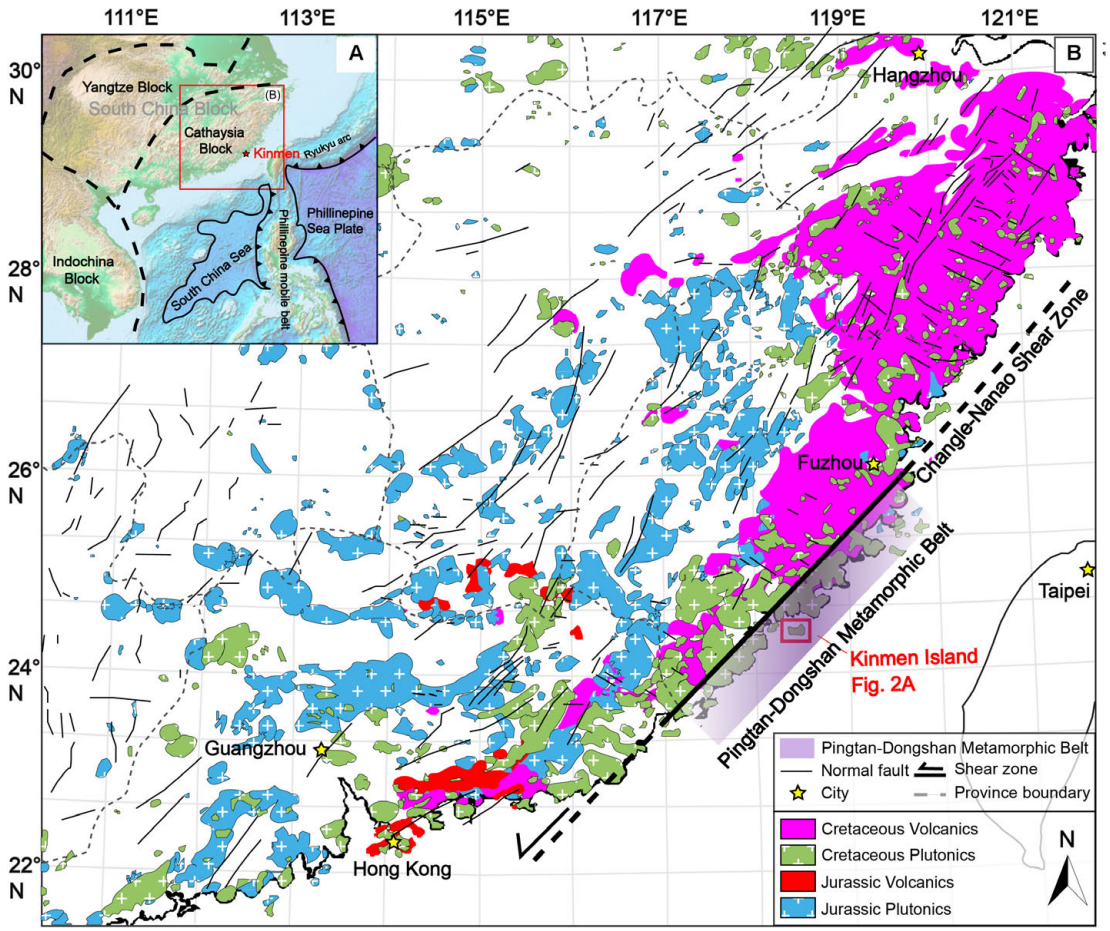

FIGURE 1 | Simplified tectonic and geological map of southeast Asia. **(A)** Topography map showing tectonic components of southeast Asia under present-day configuration. The black dashed lines mark the boundaries of the tectonic blocks while the black solid lines mark the boundaries between continental crust and oceanic crust. Solid black lines with triangles indicate the subduction zones. **(B)** Geological map modified and compiled from Li J. et al. (2014) and Zhou et al. (2006) illustrating the distribution of the Jurassic and Cretaceous plutonics and volcanics, Mesozoic normal faults, Changle-Nanao Shear Zone (CNSZ), and the Pingtan-Dongshan Metamorphic Belt (PDMB). The red rectangle indicates the study site in this study.

geobarometer (Lo et al., 1993). Combined with the upper crustal intrusion of the mafic dike swarms, Lin (1994) concluded the continental crust of the Kinmen Island underwent thinning and the exhumation of the lower crustal granitoids. To decipher more detailed history of crustal extension as well as the plate interactions, it is crucial to understand the structural evolution of the metamorphosed and highly deformed units, which has been omitted from previous studies. Hence, detailed outcrop mapping, structural measurements and petrographic analysis in the Kinmen Island were conducted.

RESULTS AND INTERPRETATION

Field and oriented thin section analysis were conducted from 14 sites, which are divided into two groups according to their exhumed batholiths (**Figures 2**, **3**). One belongs to the Taiwushan Granite, including Fu Guo Duen (FGD), Dong Cun (DC), Nan Shih Hu (NSH), Liang Jin Farm (LJF), Tai Hu Road (THR), Gung Yan Road (GYR), Kinmen Botanical Garden (KBG), Huan Jung Road (HJR), Ma Shan (MS), Han She Hua (HSH), and Zhain Shan (ZS). The other falls into the Chenggong Tonalite, encompassing Hou Bian (HB), Tien Pu (TP), and Cheng Gong (CG) (**Figure 2**). A total of 568 structural measurements were taken (**Figure 3** and **Supplementary Table S1**) with three oriented samples analyzed for petrography. There are two newly identified rock units in this study: the amphibolite schist and garnet-bearing leucogranite (**Figure 4**). The amphibolite schist is only confined within the Chenggong Tonalite as abundant xenoliths, which records the same deformation history as the country rocks (**Figure 4B**). The garnet-bearing leucogranite was previously considered to be the differentiates of the Tienpu Granite (Lin et al., 2011); however, we now considered it to be an independent rock unit because it not merely was deformed during D_2 and D_3 but also intruded by the Tienpu Granite (**Figure 4F**).

Based on the crosscutting relationships of fabrics and lithology units in the field and oriented thin sections, we recognized

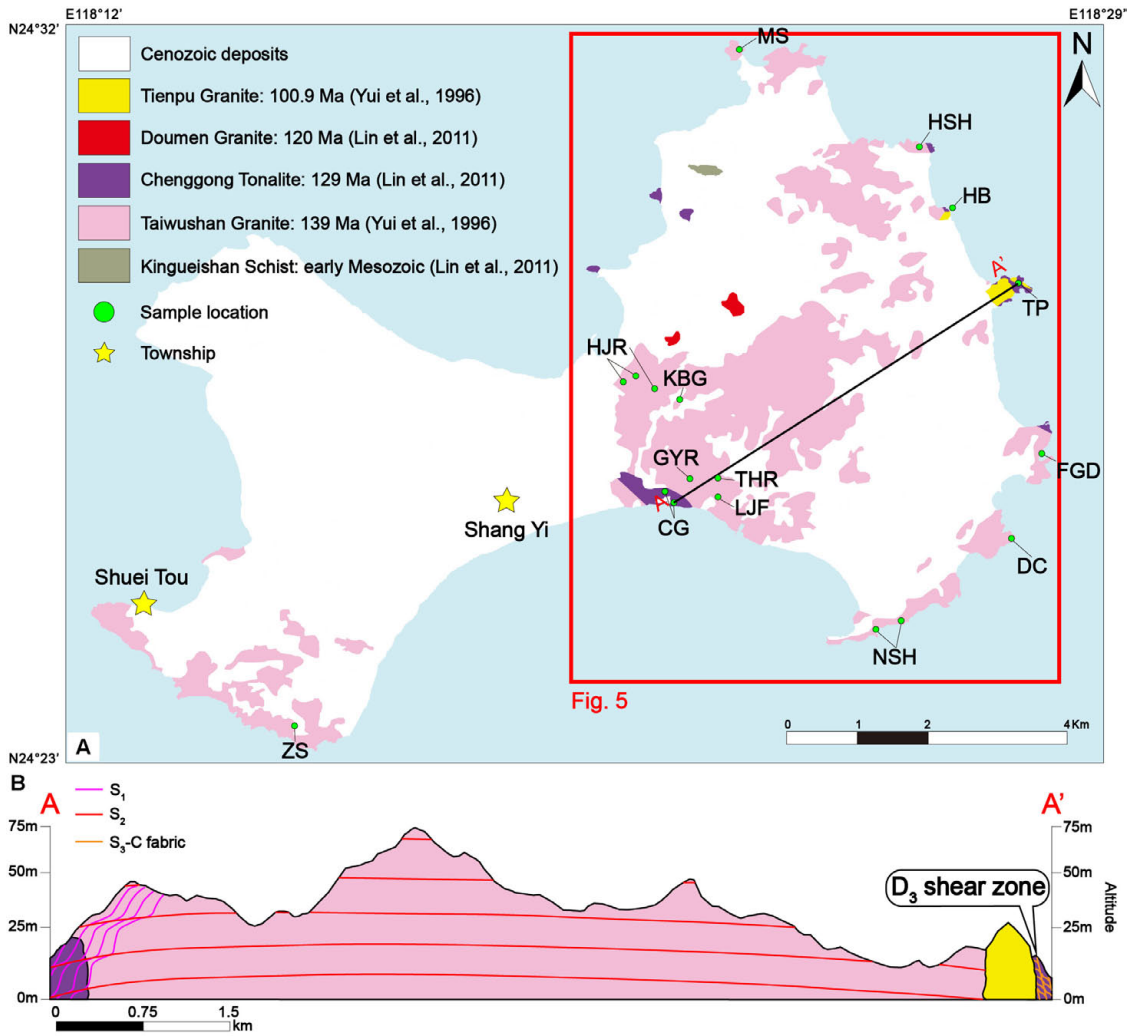

FIGURE 2 | Geological map of the Kinmen Island showing the distribution of Cretaceous magmatism and sample locations. **(A)** Geological map modified from Lin et al. (2011). **(B)** Schematic diagram of reconstructed A-A' cross section. The pink line indicates the gneissic foliation (S_1) defining the D_1 doming event. The red line indicates the subhorizontal S-tectonite (S_2) of D_2. The orange line indicates the locally developed D_3 shear belts (S/C fabric).

five deformation events and five magmatic events combining all study sites. The Taiwushan Granite, Chenggong Tonalite, and amphibolite schist xenoliths record all the deformation events (D_1–D_5; **Figures 2–8**). The magmatism of garnet-bearing leucogranite (G_2) persisted from pre-D_2 to post-D_3 (**Figures 4C,F**, **6E**, **7D,E,I**). The undeformed Tienpu Granite (G_3) crosscuts the Chenggong Tonalite and garnet-bearing leucogranite, which marks the end of all the ductile deformation events (D_1–D_3) at 100.9 Ma (age from Yui et al., 1996; **Figures 2B**, **4D,F**). With the age of 129 Ma reported for the Chenggong Tonalite by Lin et al. (2011), we constrain the D_1–D_3 ductile deformation events between 129 and 100.9 Ma. Both G_2 and G_3 have close spatial relationship to the distribution of D_3 shear belts. The D_4 and D_5 are K-feldspar-quartz ± biotite pegmatitic dykes (G_4) and mafic dykes (G_5) following brittle factures (**Figures 4G,H**, **8**). Our petrography analysis and field observation indicate that the metamorphic condition retrograded from the granulite facies (D_1), to the upper- to middle-amphibolite facies (D_2–D_3), and finally into the greenschist facies (D_4–D_5). The results of reconstructed evolution are described below.

D_1

D_1 is a kilometer scale gneiss-dome structure with the Chenggong Tonalite skirting the central Taiwushan Granite at the southwest and northeast margin (at CG, FGU, TP, HB, and HSH locality of **Figures 2**, **5**). Moderately to shallowly dipping gneissic foliation (S_1) were formed around the margin of Taiwushan Granite and within the Chenggong Tonalite, all of which dip away from the core of Taiwushan Granite (**Figures 2B**, **3**, **5**). The moderately to shallowly down-dipping mineral stretching lineation was mainly developed at the southwest, south and southeast side of the Taiwushan Granite at CG, NSH, and DC, respectively (**Figure 5**). The south

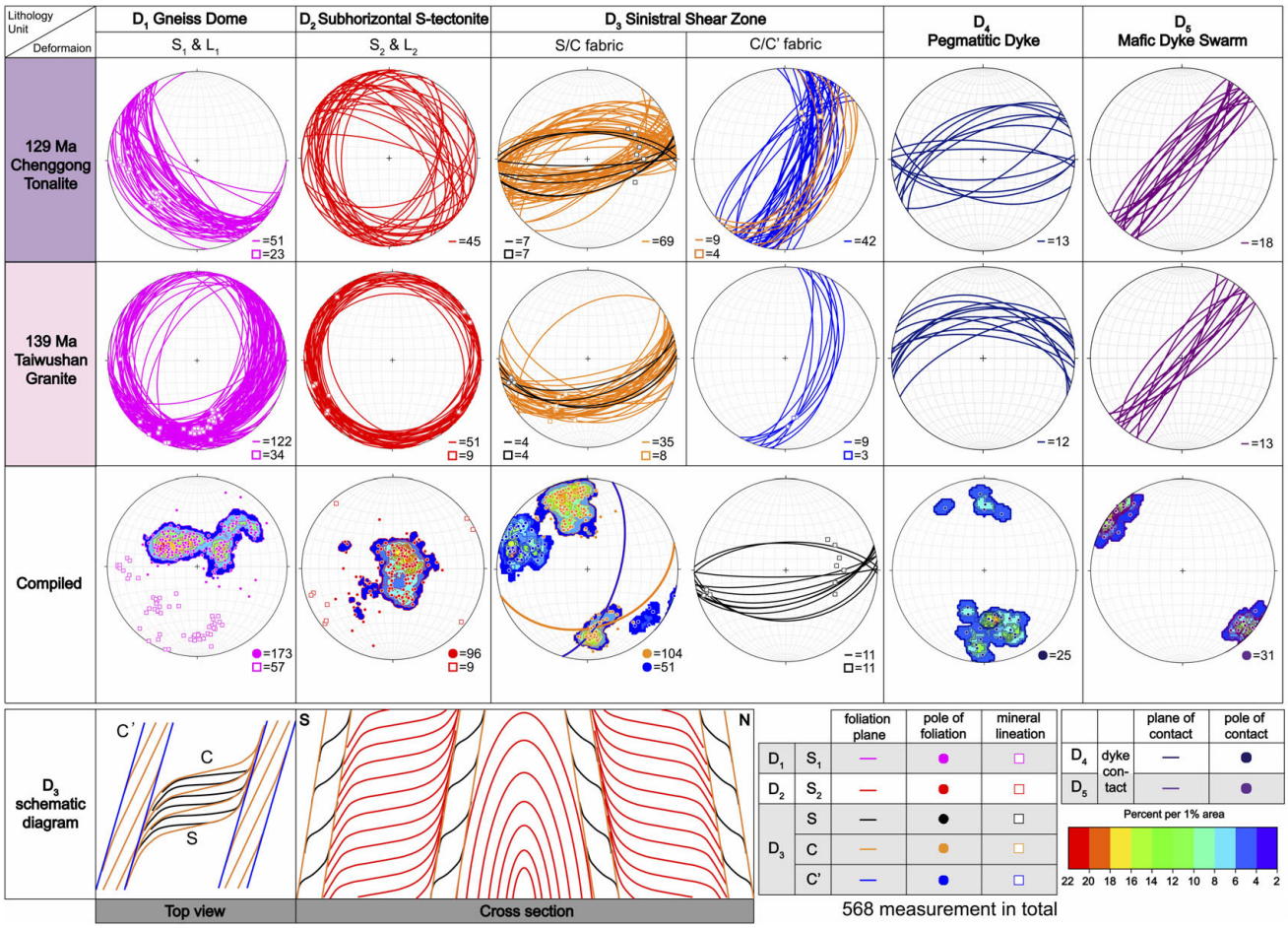

FIGURE 3 | Equal-area southern hemisphere stereographic projections of structure measurement data from 139 Ma Taiwushan Granite and 129 Ma Chenggong Tonalite with D_3 schematic diagrams showing the structural relationships of D_2 and D_3 as well as S/C/C' fabrics. Different colors represent different deformation fabrics. The pole of foliation is used to show the compiled structure data. The mean plane of the D_3 fabric (C and C' surface) is plotted. The measurement data can be found in **Supplementary Table S1**.

limb of the dome is characterized by L-S tectonite with W-, SW- to S-plunging lineation indicative of non-coaxial strain, while S-tectonite is the feature of the east and west side of the dome at FGD and HJR locality suggestive of the flattening strain (**Figures 3**, **5**). It is implied that the strain state was mainly non-coaxial at the southwest, south and maybe northeast side of the Taiwushan Granite. This idea is further supported by the intrusion location of the Chenggong Tonalite and the development of the D_3 shear belt at the northeast side of the dome.

In the field at CG, the S_1 foliation is accompanied with *in situ* partial melting of the Chenggong Tonalite, which sets the peak metamorphic condition of D_1 as the granulite-facies (**Figure 6A**). The S_2-folded leucocratic melt further constrains this migmatitic condition only during D_1 event (**Figure 6B**). Petrographically, S_1 is defined by the alignment of subhedral biotite at the cleavage domain, whereas elongated quartz, aligned feldspar and anhedral hornblende within the microlithon domain (sample 1118CG01; **Figure 9**). Other than foliation-defining biotite, randomly oriented anhedral biotite and euhedral epidote can also be observed within the microlithon domain. The random orientation of anhedral biotite and hornblende within microlithon domain suggests they are igneous relicts. The foliation-defining biotite are often in contact with hornblende indicating these coarser subhedral biotite grains are new metamorphic minerals grown by fluid-and-deformation-facilitated metamorphic reaction under the amphibolite facies condition (Berger and Stünitz, 1996). Apart from hornblende to biotite and epidote reaction, grain boundary migration (GBM) with dynamic inter-fingering growth, chessboard extinction of quartz can be observed indicating deformation temperature for D_1 should be above 630°C (Stipp et al., 2002). The feldspars are deformed mainly by sub-grain rotation recrystallization (SGR) and bulging (BLG). The presence of myrmekite between the grain boundaries of plagioclase and K-feldspar indicates the occurrence of K-metasomatism during deformation (**Figure 9B**). These mineral assemblages and crystallographic deformation conditions suggest D_1 persisted from the granulite facies to the

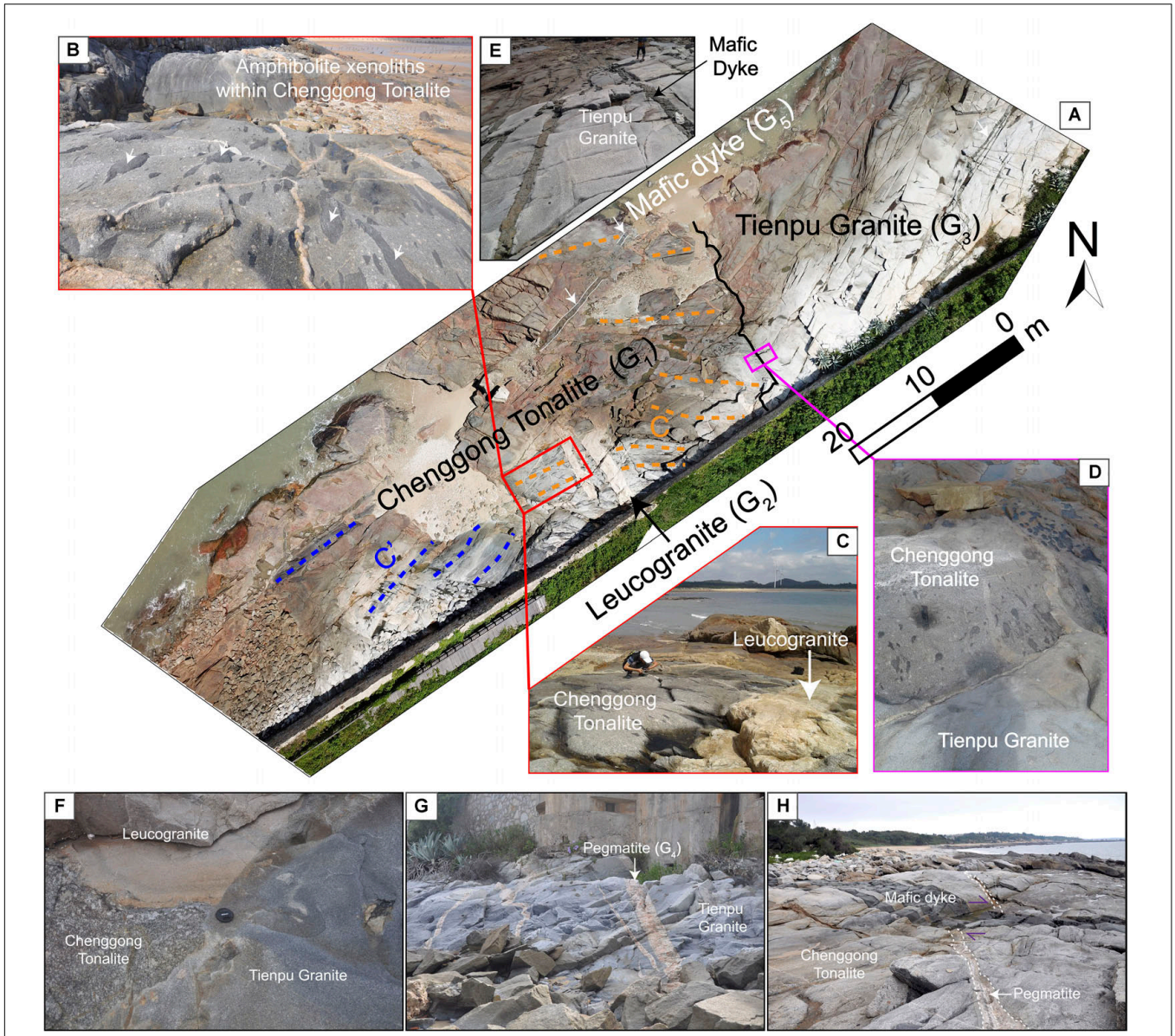

FIGURE 4 | Aerial and outcrop photos of Tien Pu (TP) region showing the crosscutting relationships of different lithology units (G_1–G_5). **(A)** Aerial photo of part of the TP region with sketched D_3 C/C' fabrics and labeled lithology units of Chenggong Tonalite (G_1), leucogranite (G_2), Tienpu Granite (G_3), and mafic dykes (G_5). **(B)** Deformed Chenggong Tonalite with aligned amphibolite schist xenoliths that are heterogeneously deformed and sheared. **(C)** Deformed Chenggong Tonalite intruded by post-D_3 leucogranite. **(D)** Deformed Chenggong Tonalite intruded by undeformed Tienpu Granite. **(E)** Undeformed Tienpu Granite truncated by the mafic dike. **(F)** Chenggong Tonalite intruded by leucogranite, both of which are truncated by Tienpu Granite. **(G)** Tienpu Granite intruded by pegmatites (G_4). **(H)** Pegmatites crosscutted and dextrally displaced by the mafic dike.

upper amphibolite facies. Post D_1 retrograde chlorite replacing hornblende and biotite can also be observed.

D_2

D_2 formed subhorizontal S-tectonite with little to none mineral lineation as the D_1 gneiss dome further exhumed (**Figures 3**, **6F**). The S_2 gneissic foliation distorted the S_1 doming fabrics into wavy foliations indicative of crustal extrusion from the core of Taiwushan Granite to the margin (**Figures 5B**, **6C,D**). The vertical shortening stress is suggested by the flattening strain of the subhorizontal S-tectonite. The S_2 foliation was well-developed at the northeast side of the dome with S_1 doming fabrics all transposed and unobservable within both the Taiwushan Granite and Chenggong Tonalite (e.g., HSH and TP; **Figures 7D,I**). In contrast, the S_2 fabric is confined to a discrete, centimeter-scale zone with wavy S_1 doming foliations preserved at the other parts of the dome margin (e.g., CG and FGD; **Figures 5B**, **6C,D**). The stronger and more penetrative S_2 fabric development at the northeast side of the dome reveals the strain partitioning and strain concentration

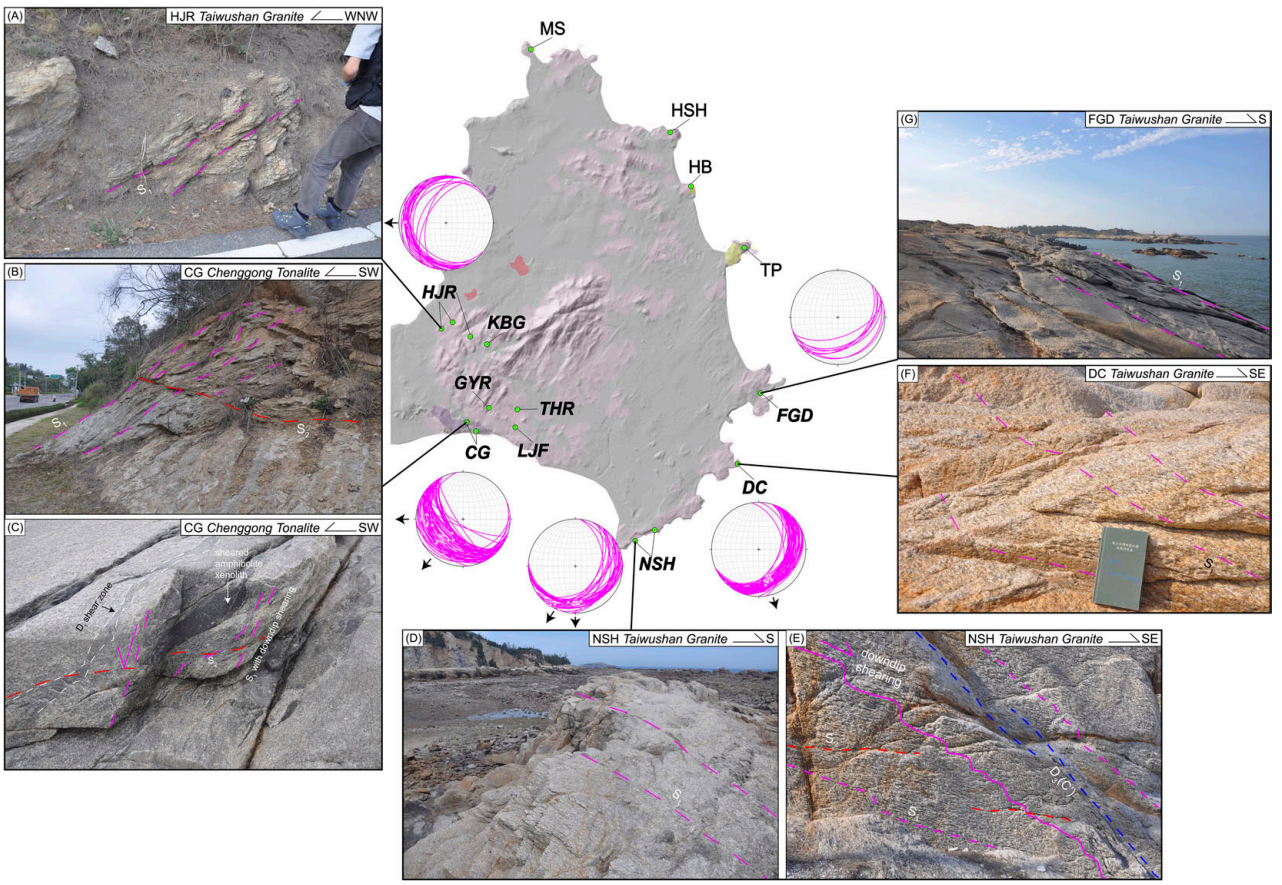

FIGURE 5 | Topographic map overlaid by the geological map showing outcrop photos with measured S_1 gneissic foliation and mineral lineation plotted with equal area southern hemisphere stereonet projection to demonstrate D_1 gneiss dome. The bold italic words indicate the sample locations with S_1 fabrics preserved. **(A)** The N-S striking and shallowly W-dipping gneissic foliation with poorly to none mineral lineation developed at HJR. **(B,C)** The NW-SE striking, shallowly to moderately SW-dipping gneissic foliation (S_1) with well-developed W and SW plunging lineation at CG. The S_1 fabric is deformed into a wavy form due to the subhorizontal S_2 foliation. The sheared amphibolite xenolith indicates the down-dip shearing along the S_1 foliation. **(D,E)** The NE-SW striking, shallowly to moderately SE-dipping gneissic foliation (S_1) with well-developed SW and S plunging lineation at NSH. The kinking of S_1 foliation is owing to the weak development of the subhorizontal S_2 foliation, both of which are crosscutted by D_3 shear zone (C' fabric). **(F)** The NE-SW striking, moderately SE-dipping gneissic foliation (S_1) with well-developed SSE plunging lineation at DC. **(G)** The ENE-WSW striking, moderately SE-dipping gneissic foliation (S_1) with none lineation developed at FGD.

at the northeast side of the gneiss dome. In addition, the subhorizontal foliation can be traced continuously at the same height level with the core of meter-scale thickness and the margin of centimeter-scale (**Figures 6C,D,F**). It's suggested that the vertical shortening stress was more concentrated in the core of Taiwushan Granite in the hint of the vertical movement of the gneiss dome as evidenced by the kink fold of S_1 fabric at the NSH locality (**Figure 5E**).

The S_2 folded leucocratic melt and lack of migmatite in the D_2 domain imply the peak deformation condition of D_2 was below granulite facies condition (**Figure 6B**). Similar to D_1, the S_2 foliation is defined by elongated quartz, feldspar ribbons, euhedral to subhedral biotite and subhedral to anhedral hornblende folia (**Figure 10**). The deformation mechanism of quartz is mainly of GBM and even chessboard extinction suggestive of peak deformation temperature >630°C (**Figures 10A,B**; Stipp et al., 2002). Both K-feldspar and plagioclase augens were deformed by SGR. The peak deformation condition of D_2 can be constrained to the upper amphibolite facies.

D_3

D_3 is a ENE-WSW striking subvertical sinistral shear zone forming S/C/C' fabrics and shear folds with regional heterogeneous strain partitioning ranging from centimeter-scale to a-hundred-meter scale (**Figure 7A**). The centimeter-scale mylonite belt are observed at the core (e.g., THR; **Figure 7B**), and along the margin of the Taiwushan Granite (e.g., NSH and FGD; **Figure 7C**). At the northeast limb of the dome (HSH, HB, and TP), D_3 is characterized by a-hundred-meter scale mylonite belt with locally preserved S_2 fabric and folded pre-D_3 leucogranitic dike (**Figures 7D,I**). The S/C/C' fabric, σ-type feldspar augens, shear folding along the S fabric indicate the sinistral shear sense of the shear zone (**Figures 7F–H**). The S/C/C' fabric can be noted from the amphibolite schist xenolith, Chenggong Tonalite, and Taiwushan Granite (**Figures 7F,H, 11A,D**).

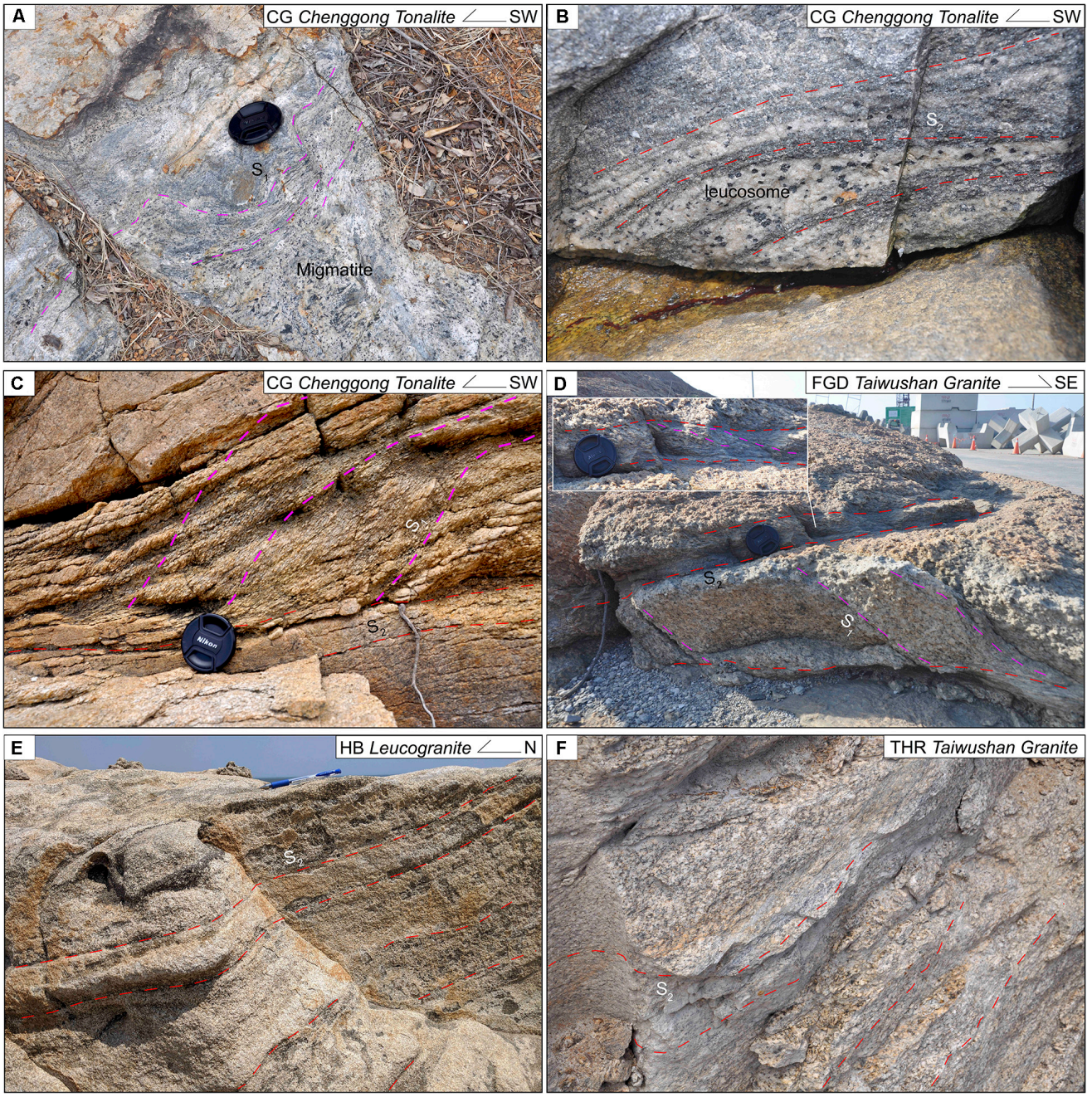

FIGURE 6 | Outcrop photos and sketches showing interpreted structures of D_1 and D_2. **(A)** *In situ* migmatite developed along the S_1 gneissic foliation within Chenggong Tonalite at CG. **(B)** S_2-folded leucosome in Chenggong Tonalite indicates that the migmatitic condition is confined in D_1 domain at CG. **(C)** Wavy S_1 foliation due to the development of subhorizontal S_2 foliation at CG. **(D)** Subhorizontal S_2 foliation crosscuts the S_1 doming fabric in Taiwushan Granite at FGD. **(E)** Subhorizontal S_2 foliation developed within the leucogranite showing the pre-D_2 magmatic intrusion at HB. **(F)** Subhorizontal S_2 foliation (S-tectonite) developed in Taiwushan Granite at THR.

The mineral stretching lineation and the D_3 fold axis show two dominant orientations: one plunges toward the north to east quadrant, while the other plunges toward west to south quadrant (**Figures 3**, **7A**). Combining with the sinistral sense of shear, the N- to E-plunging lineation reveals a transtensional nature for the shear belt. Although the W- to S-plunging lineation reveals transpressional nature, it was possibly due to heterogeneous strain localization effect. Of all outcrops other than HB and NSH indicate transtentional deformation environment of D_3.

The foliations observed from the Chenggong Tonalite are defined by the alignment of subhedral to anhedral hornblende,

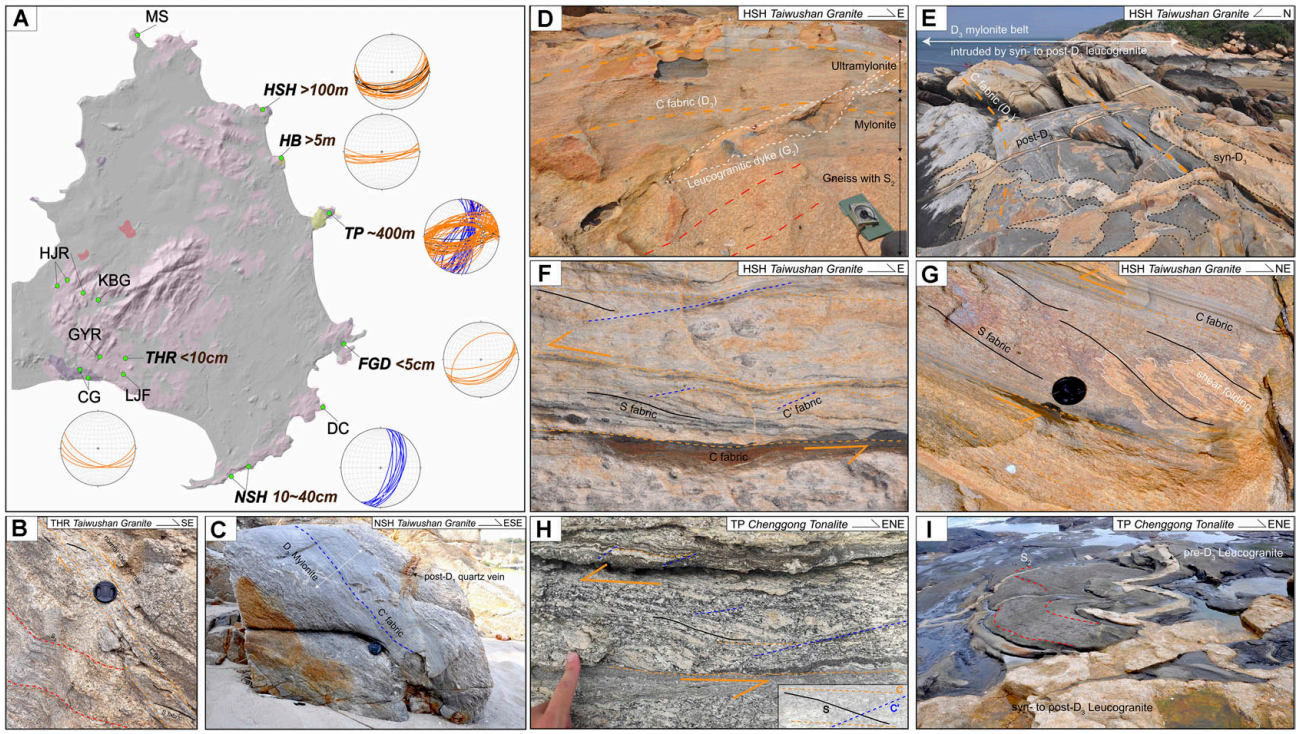

FIGURE 7 | Topographic map overlaid by the geological map showing outcrop photos with measured D_3 shear fabrics and mineral lineation plotted with equal area southern hemisphere stereonet projection. The bold italic words indicate the sample locations with D_3 shear fabrics identified. **(A)** Topographic map with geological map showing the sample locations with D_3 shear zone developement. The brown numbers show the width of the shear zone. **(B)** S/C fabric with normal shear sense crosscuts the subhorizontal S_2 foliation within Taiwushan Granite at THR. **(C)** D_3 mylonite (C' surface) crosscuts the post-D_1 quartz vein within Taiwushan Granite at NSH. **(D)** D_3 shear zone (C fabric) development from mylonite to ultramylonite crosscutting the S_2 fabric, both of which are intruded by leucogranitic dike (G_2) within Taiwushan Granite at HSH. **(E)** D_3 mylonite belt intruded by syn- to post- D_3 leucogranite (G_2) within Taiwushan Granite at HSH. **(F)** S/C/C' fabric showing sinistral shear sense within Taiwushan Granite at HSH. **(G)** S/C fabric indicating sinistral shear sense with shear folding along the S fabric within Taiwushan Granite at HSH. **(H)** S/C/C' fabric showing sinistral shear sense within Chenggong Tonalite at TP. **(I)** Subhorizontal S_2 fabric and pre-D_3 leucogranite (G_2) folded during D_3, both of which are intruded by syn- to post-D_3 leucogranite (G_2) at TP.

elongated quartz ribbons, and biotite folia (**Figures 10C**, **11D**). The deformation mechanisms observed from quartz are mainly GBM without chessboard extinction, which indicates the deformation temperature during shearing should range between 550 and 630°C. This is further supported as the observed K-feldspar and plagioclase was deformed mainly by SGR, and the precipitation of myrmekite along the K-feldspar grain boundaries (**Figure 11E**). The S/C/C' fabrics are better preserved within the amphibolite xenolith as the grain size are much finer than that of the Chenggong Tonalite. Two generations of hornblende can be noted, as one is the igneous relict (anhedral with green color, Hb1) and the other is the syn-D_3 metamorphism (euhedral to subhedral with yellow color, Hb2; **Figures 11A,B**). The new growth of metamorphic amphibole indicates the D_3 shearing event occurred under middle to lower amphibolite facies condition. Aside from the high-temperature deformation features, most quartz and feldspar have granoblastic polygonal texture showing annealing effect after the shearing event (**Figure 11C**). Based on that, we suggest the metamorphic temperature was still $\geq$400°C post D_3 shearing event. Greenschist-facies retrograde mineral assemblage of chlorite and epidote overprinted the biotite and hornblende, indicating that retrograde metamorphism occurred post D_3 (**Figures 11C,F**).

D_4 and D_5

D_4 is defined by the intrusion of the Tienpu Granite (G_3) followed by E-W striking, both N and S steeply dipping pegmatites (G_4; **Figures 4G,H**, **8A**). After the intrusion of the Tienpu Granite (G_3), no ductile deformation is noted. The pegmatite intrusion (G_4) is accompanied by sinistral displacement as they truncate and sinistrally offset the D_3 mylonite belts (**Figure 8A**). Greenschist facies mineral assemblages of chlorite, epidote and sericite are noted under thin section (**Figures 11C,F**). The retrograde replacement of biotite and hornblende to chlorite and epidote (**Figure 11**) further supports the lower temperature condition should be reached post D_3. The youngest deformation event (D_5) was NE-SW striking subvertical mafic dike swarms (G_5), which crosscuts all the magmatic rock units (G_1–G_4) and D_1–D_3 fabrics (**Figures 3**, **4A,E,H**). The mafic dike intrusion is accompanied by dextral displacement shown by the displaced D_4 pegmatite and the dextral fault displacing the aplitic dykes (**Figures 4H**, **8B**). The brittle nature of the basaltic dike intrusion indicate the temperature condition for D_5 should

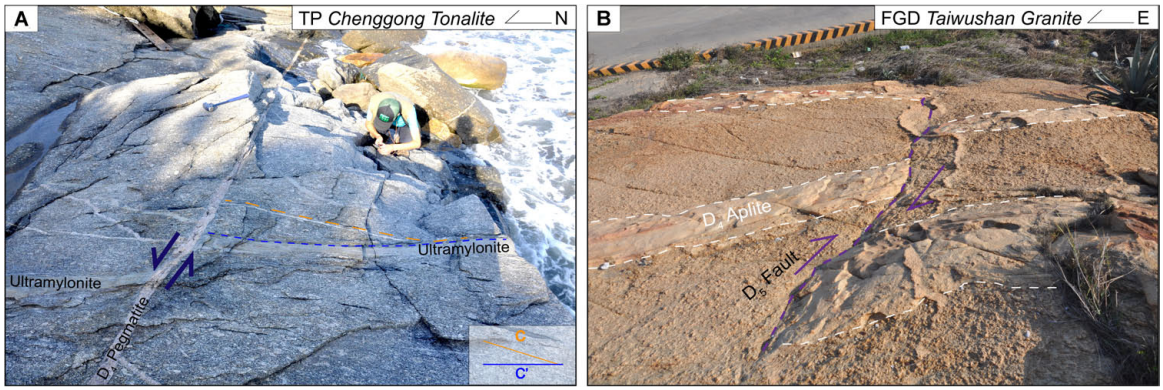

FIGURE 8 | Outcrop photos and sketches showing interpreted structures of D_4 and D_5. **(A)** D_4 pegmatite sinistrally displaced the Chenggong Tonalite with C/C' fabric, suggested by the displaced ultramylonite. **(B)** D_5 fault dextrally displaced the D_4 aplite.

also be under the lower greenschist facies, and was close to the ground surface.

DISCUSSION

Thermochronological Constraints on the Reconstructed Structural Evolution

Based on the crosscutting relationship observed in the field and oriented thin sections, three ductile deformation events (D_1, D_2, D_3) are reconstructed from both the Taiwushan Granite and the Chenggong Tonalite. These ductile events were followed by three magma intrusion under brittle condition (D_4/G_3, G_4, and D_5/G_5). The timing of D_4 and D_5 can be readily allocated to the crystallization ages of the magmatism, which are ca. 100 Ma (Yui et al., 1996) and between 90 and 76 Ma (Lee, 1994), respectively. Among these structural and magmatic intrusion events, the crystallization ages of the deformed Taiwushan Granite (139 Ma, Yui et al., 1996), the Chenggong Tonalite (129 Ma, Lin et al., 2011), and the undeformed Tienpu Granite (100 Ma, Yui et al., 1996), provide a rough time constraint for the three ductile deformation events to at 129–100 Ma. However, to establish the detailed timing of each deformation event, further work of $^{40}Ar/^{39}Ar$ geochronology, petrography and P-T estimates of these rocks are required.

$^{40}Ar/^{39}Ar$ thermochronology has been widely utilized to investigate the timing, rates and durations of deformation events (e.g., Wang and Lu, 2000; Chen et al., 2002; Chiu et al., 2018). Such study was uncommonly applied for the structural evolution of Cretaceous batholiths along the coast of SE Asia (Wang and Lu, 2000; Chen et al., 2002). One major reason is that the deformation events were interpreted as syn-magmatism, hence zircon U-Pb geochronology was dominantly employed to decipher the structural evolution (Tong and Tobisch, 1996; Shi, 2011; Li et al., 2015). To better constrain the timing of our reconstructed deformation events of the Kinmen Island, the available $^{40}Ar/^{39}Ar$ geochronology data are compiled and discussed below (**Figure 12**).

Lo et al. (1993) conducted $^{40}Ar/^{39}Ar$ geochronology for the Taiwushan Granite and reported plateau ages of 100.2 ± 0.9 Ma for hornblende separates (green square within **Figure 12A**) with estimated closure temperature of 557 ± 7°C, and 97.4 ± 0.9, 97.2 ± 0.9 Ma for biotite separates with estimated closure temperature of 333 ± 4°C and 292 ± 3°C (brown squares within **Figure 12A**). Complex age spectrum with a minimum age of 80 Ma in low-temperature steps that become older to a maximum of 90 Ma in high-temperature steps were reported for K-feldspar separates with closure temperature being estimated to 292 ± 3°C (Figure 2C within Lo et al., 1993). In addition, Lin (1994) analyzed the K-Ar ages of biotite and K-feldspar separates from both the Taiwushan Granite and Chenggong Tonalite. The acquired ages for biotite were 93.0 ± 2.0 and 94.1 ± 2.0 Ma and for K-feldspars are 90.9 ± 2.0 and 84.5 ± 1.8 Ma.

By plotting reported $^{40}Ar/^{39}Ar$ ages according to their estimated closure temperature, two cooling paths can be constructed. One is for the ductile deformed Taiwushan Granite and Chenggong Tonalite from 129 Ma (pink dash line in **Figure 12A**), while the other is for the undeformed Tienpu Granite since 100 Ma (yellow dash line within **Figure 12A**). Our petrological and microstructural analyses indicate upper amphibolite facies (≥630°C) metamorphic condition for D_1 and D_2. As we correlate the reconstructed cooling curve to 630°C, 107 Ma marks the boundary between D_2 and D_3 (**Figure 12A**). Similarly, as we correlate the temperature range of granulite facies (≥700°C) of D_1, a range between 129 and 114 Ma can be inferred (**Figure 12A**). The D_4 Tienpu Granite (100 Ma) crosscutting all foliations marks the termination of D_3, and the initiation of D_4. The brittle nature of D_4 and D_5 indicate the metamorphic condition are at shallow crustal level close to the surface. The low temperature condition (150–400°C) of the reconstructed cooling path and the presence of retrograde mineral assemblages further support the reconstructed temperature evolution.

The deformed Taiwushan Granite and Chenggong Tonalite underwent a rapid cooling from 550 to 300°C around 100 Ma. Similar rapid cooling rate is noted for the Tienpu Granite since 100–90 Ma (200°C). It's indicated that the crystalline rock was uplifted by about 12 km during that time (average

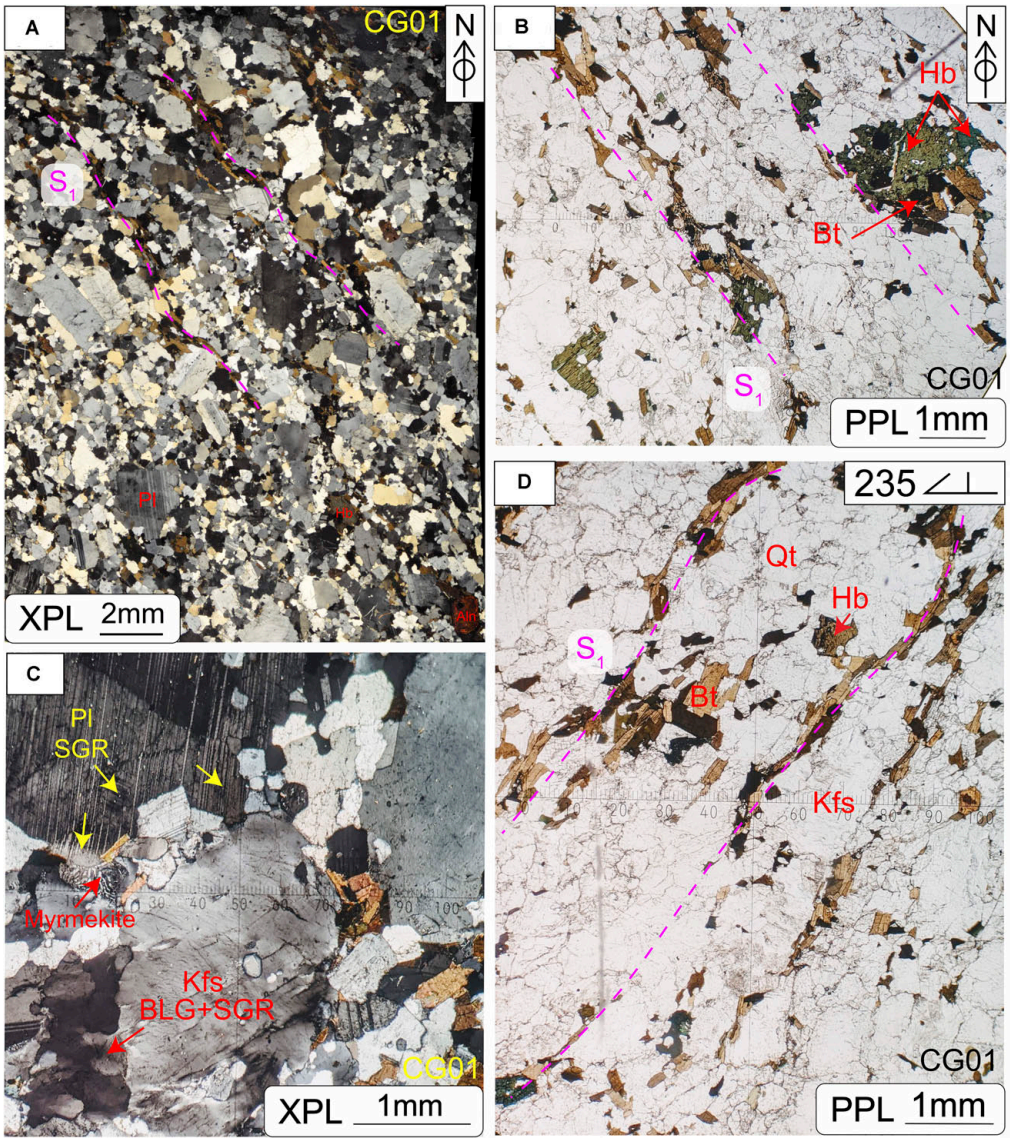

FIGURE 9 | Microphotographs showing microstructures and petrographic relationship of D_1. **(A)** S_1 foliation defined by alignment of biotite, elongated quartz, and plagioclase. The weak development of foliation is due to the low percentage of biotite in the sample and the granoblastic interlobate texture developed in the granulite facies condition. **(B)** Myrmekite precipitated between the K-feldspar and plagioclase, which is post the granoblastic interlobate matrix of quartz and feldspar aggregates. The deformation mechanism is SGR and BLG for K-feldspar, and SGR for plagioclase. **(C,D)** Gneissic layering suggested by the biotite cleavage domain and the quartzofeldspathic microlithon domain. Hb-hornblende; Bt-biotite; Pl-plagioclase; Aln-allanite; SGR-subgrain rotation recrystallization; BLG-bulging.

crustal geothermal gradient 25°C/km) revealing an average uplifting rate of 12 mm/a. Such rapid cooling rate can not be explained by the magma cooling alone. Blythe (1998) examined the surface uplift rates under different tectonic settings utilizing isotopic and fission track analysis, and revealed a surface uplift rate of 5–10 mm/a for active contraction region such as the Himalaya and Southern Alps in New Zealand. A much less surface uplift rate of ∼7 mm/a was obtained for the active extension region, such as for the D'Entrecasteaux Islands and Papua New Guinea. An even smaller uplift rate of 1–5 mm/a was obtained along the restraining bends of San Andreas strike slip fault systems. According to our reconstruction, this rapid cooling resulted from D_3 transtensional shearing. If we combine the uplift rate for the extension and strike-slip region, an 8–12 mm/a uplift rate is inferred, which is similar to what the cooling path suggests. The transtensional shearing can not only produce free space for later magma emplacement (Tienpu Granite), but also trigger larger vertical displacement. Taking the transtensional shearing and the denudation of the brittle upper crust induced by crustal extension into combination, such a rapid cooling rate is acquired around 100 Ma. This idea is further supported by the $^{40}Ar/^{39}Ar$ ages of the rocks within the PDMB [the sample of FJ07, FJ08, FJ12, and FJ17 in Chen et al. (2002); **Figure 12B**]. It's shown that the rapid cooling from the

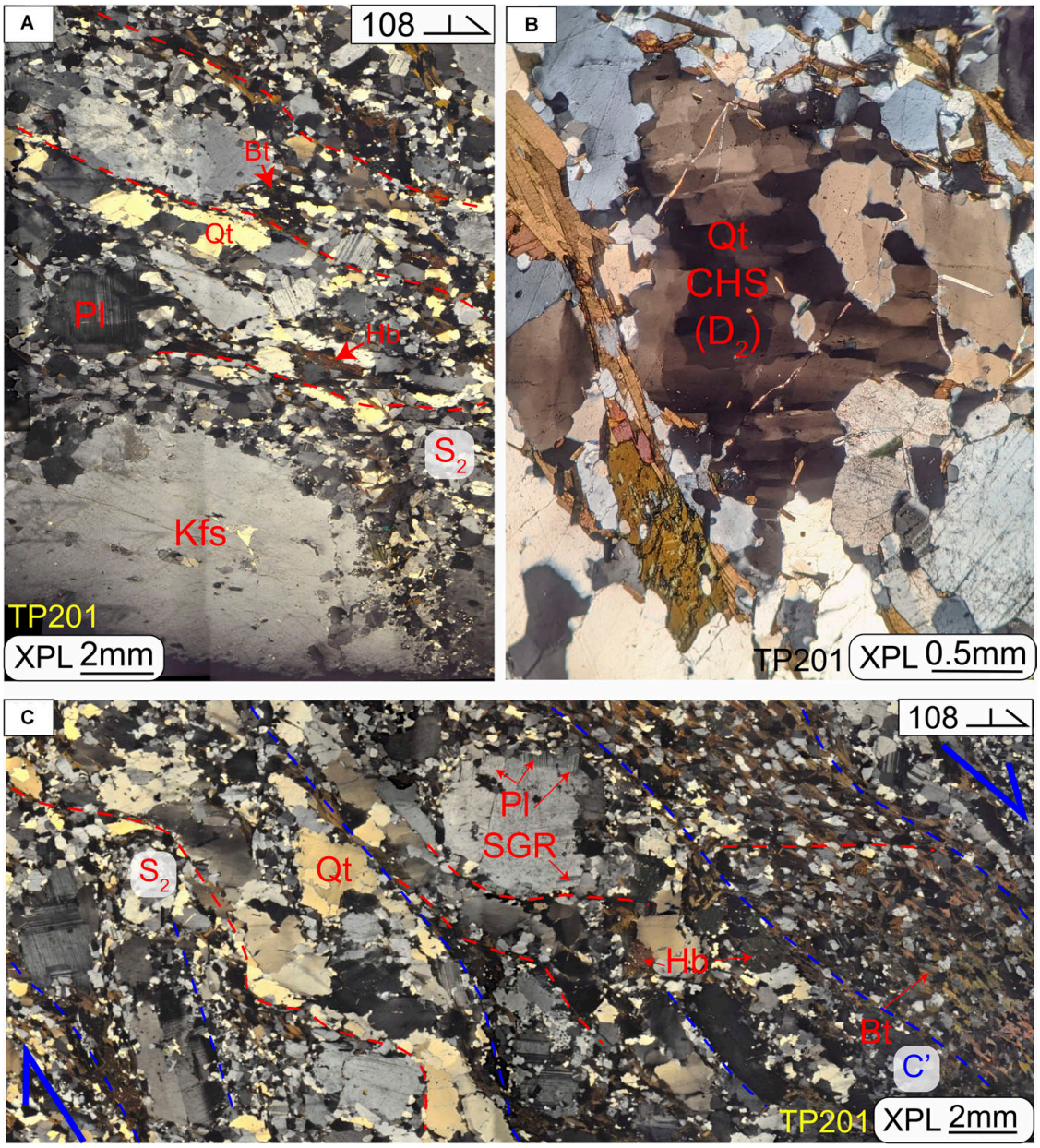

FIGURE 10 | Microphotographs showing microstructures and petrographic relationship of D_2 and D_3. **(A)** S_2 foliation defined by alignment of biotite, elongated quartz, feldspar, and hornblende. The K-feldspar porphyroclasts are mainly deformed by SGR and BLG with myrmekite along the margin. The plagioclases are recrystallized with granoblastic polygonal texture and SGR within the microlithon domain. The quartzs are deformed mainly by grain boundary migration (GBM). The deformation mechanisms of these quartz-feldspar aggregates suggest upper amphibolite facies condition. **(B)** Chessboard extinction of quartz illustrating the deformation temperature is >630°C. **(C)** S_2 foliation sheared by C' fabric with normal sense of shear. D_2-domain is defined by the coarser grain-sizes of quartz-feldspar aggregates with granoblastic interlobate texture and preserved chessboard extinction within quartzs. D_3-domain (C' fabric) is defined by the finer recrystallized quartz-feldspar aggregates and biotite folia due to the shearing-induced grain size reduction.

hornblende to biotite closure temperature ranges from 109 to 90 Ma overlapping the timing of D_3 transtensional shearing and D_4 brittle fracturing, especially the clusters within D_3 events. Accordingly, the D_3 transtensional shearing along with the later brittle fracturing and accompanied denudation of upper crust could contribute to the rapid cooling during 109–90 Ma along the coast of SE Asia.

Correlation to the Structural Evolution of the Changle-Nanao Shear Zone

Other than the diachronous distribution of Cretaceous magmatism, the NE-SW striking CNSZ is another major structural feature along the coastal region of SE Asia (Chen et al., 2002; Li et al., 2015; Wei et al., 2015). By integrating data and observations in previous studies (Wang and Lu, 2000;

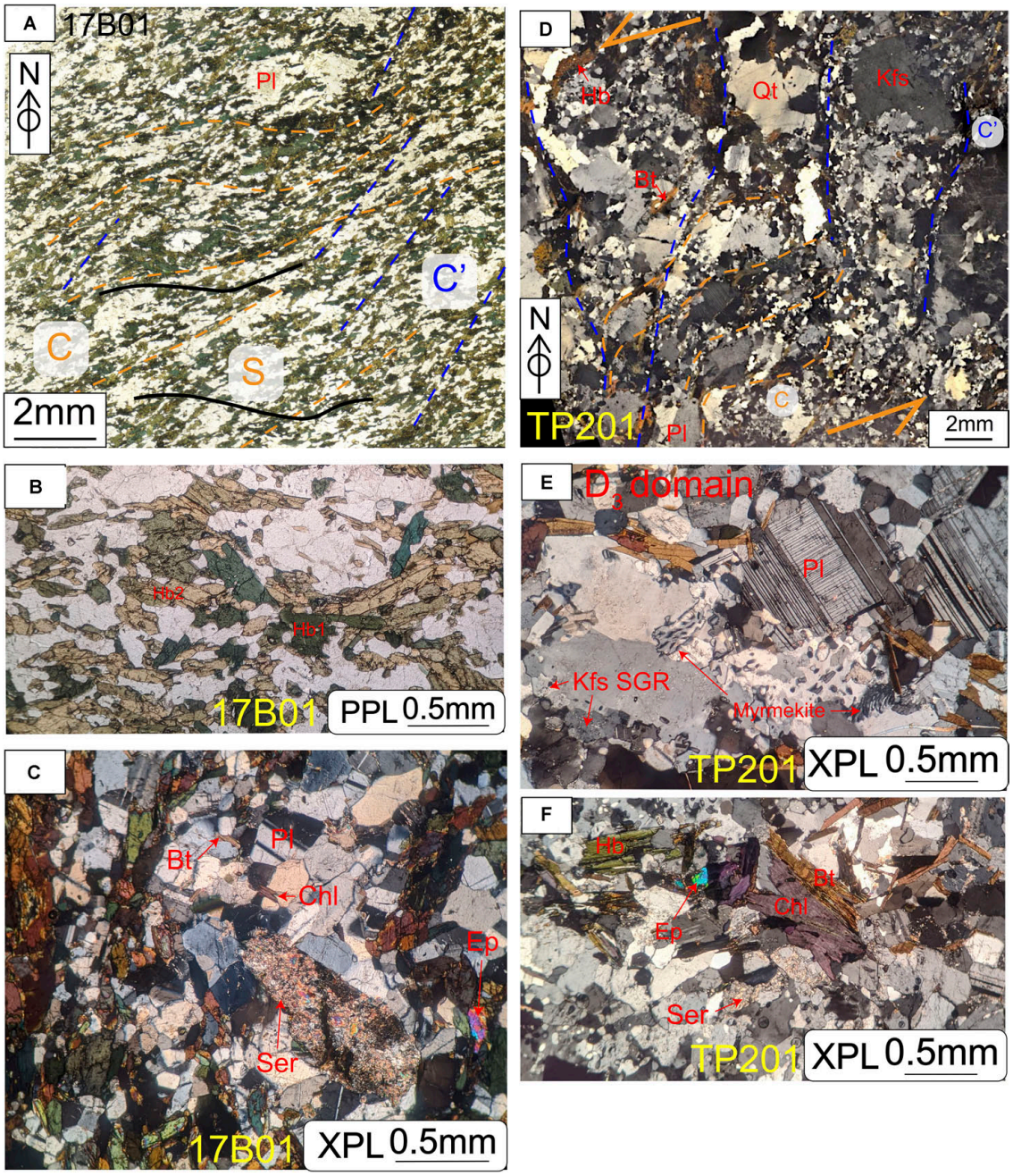

FIGURE 11 | Microphotographs showing microstructures and petrographic relationship of D_3. **(A)** S/C/C' fabric in amphibolite xenolith showing sinistral sense of shear. All fabrics are defined by the alignment of hornblende suggestive of amphibolite facies condition. **(B)** Detailed microphotograph under open nicol showing igneous hornblende (green) altered and replaced by secondary metamorphic hornblende (yellow) with granoblastic polygonal plagioclase matrix. **(C)** Granoblastic polygonal texture of plagioclase showing post-D_3 annealing with biotite growth along the plagioclase grain boundary. The retrograde overprint of the greenschist facies is shown by the chlorite, epidote and sericite. **(D)** C/C' fabric in the Chenggong Tonalite showing sinistral sense of shear. The D_3-domain is defined by the recrystallized finer-grained quartz-feldspar aggregates. The plasticity of feldspar indicated by fish structure and SGR shows amphibolite facies condition in agreement with the condition observed within amphibolite xenoliths. **(E)** Myrmekite precipitates between plagioclase and K-feldspar illustrating metasomatic process accompanying D_3 shearing. The K-feldspar is deformed by BLG and SGR. **(F)** Mineral assemblages of epidote, chlorite and sericite showing the greenschist facies post-D_3.

Shi, 2011; Wei et al., 2015), six deformation events were identified within the CNSZ based on their structural styles, metamorphic conditions and proposed relative timing. During 178–165 Ma, NE-trending foliation were developed with the amphibolite facies metamorphism (Wang and Lu, 2000). Between 149.2 and 145.4 Ma, a dextral-thrusting from NWW to SEE at lower

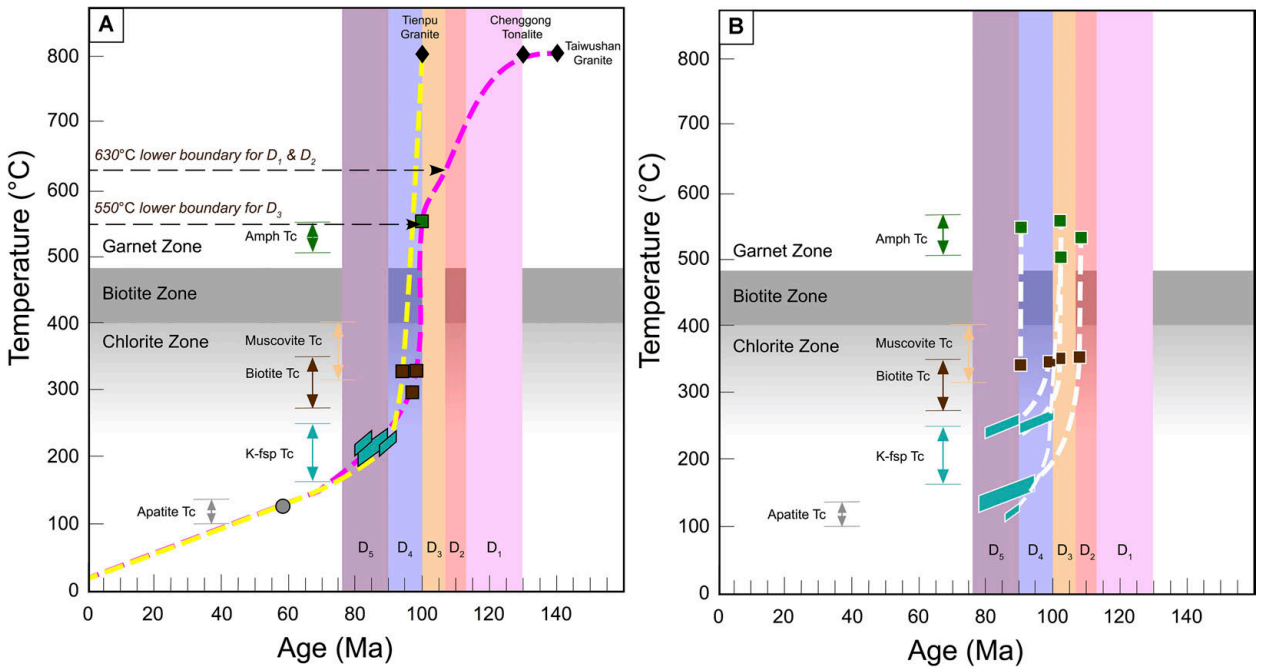

FIGURE 12 | Reconstructed cooling path of the Cretaceous magmatism of **(A)** Kinmen Island and **(B)** nearby regions based on previously published geochronological results (Lo et al., 1993; Lin, 1994; Yui et al., 1996; Chen et al., 2002; Lin et al., 2011). **(A)** The dashed pink line describes the cooling path for the 139 Ma Taiwushan Granite and the 129 Ma Chenggong Tonalite, while the dashed yellow line delineates the cooling path of the 100 Ma Tienpu Granite. **(B)** The cooling path of the gneiss within the PDMB from samples FJ07, FJ08, FJ12, and FJ17 in Chen et al. (2002). The closure temperature ranges for different mineral systems are as followed: U-Pb zircon (>800–900°C; solid black diamond Lee et al., 1997), Ar-Ar amphibole (Amph; solid green square 500–550°C; Harrison, 1982), Ar-Ar muscovite (350 ± 50°C; McDougall and Harrison, 1999), Ar-Ar biotite (275–350°C; solid brown square Döpke, 2017), Ar-Ar K-feldspar (K-fsp; solid green parallelogram 250–150°C; Harrison and McDougall, 1982), apatite fission track (110 ± 10°C; solid gray circle Gleadow and Duddy, 1981). The timing for the five deformation events (D_1–D_5) are distinguished by correlating the metamorphic conditions proposed in this study to the reconstructed cooling path.

amphibolite facies was recognized, which was followed by a sinistral-thrusting from NNW to SSE at upper-greenschist facies during 145.4–137 Ma (Shi, 2011). From 130 to 105 Ma, Wei et al. (2015) reported a northwest-directed ductile thrust with a top-to-the-NW shear sense followed by a later NE-SW folding event under amphibolite facies condition (their E1 event). During this period, Wang and Lu (2000) further separated an 118–107 Ma NE-SW trending mylonitic foliation under greenschist facies condition. Finally, a dextral strike-slip faulting with normal component at lower greenschist facies was around 100 Ma (Shi, 2011).

Compared to CNSZ, similar structural evolution of 130–105 Ma subhorizontal foliation (our D_2) followed by 118–107 Ma NE-SW mylonite belt (our D_3) and ca. 100 Ma dextral displacement (D_5) are also recognized in our study area. The structural evolution within the CNSZ from 129 Ma toward 100 Ma was generally considered to be formed under collisional setting (Li et al., 2015; Wei et al., 2015). Our data from the Kinmen Island reveals the opposite. The D_1 gneiss dome structure has never been reported previously within neither Kinmen nor CNSZ. The down-dip shearing strain pattern along the northeast and southwest limbs of this gneiss dome (**Figures 2B**, **3**), and the retrograde metamorphic conditions from granulite facies to upper amphibolite facies (**Figure 12A**) indicate extensional setting for this previously unrecognized doming event. Furthermore, despite similar subhorizontal foliations identified throughout CNSZ and Kinmen, previous researchers interpreted the origin of this subhorizontal foliation as thrust folding. Yet, according to our observation in the Kinmen island, these intervally developed subhorizontal foliations are likely generated owing to collapsing of the gneiss dome as crust further thinned (**Figure 13**). The NE-SW mylonitic foliation is also noted in the Kinmen, but it's delineated as the C' fabric of our D_3 transtensional shear belt shown by the normal shear sense (**Figure 10C**). At last, the dextral faulting can be correlated to our D_5 mafic dike swarm accompanied with dextral displacement at upper crustal level. To sum up, although similar structural evolution of D_2, D_3, and D_5 can be correlated between CNSZ and the Kinmen island, different kinematics are proposed in this study. All deformation events of Kinmen Island might have formed under extensional environment during crustal thinning. This crustal thinning event was recognized in not only the SE Asia but also the NE Asia (Sheldrick et al., 2020), which suggests the continental crust of East Asia had been thinned during the Cretaceous. Though the crustal thinning mechanism might be different among NE Asia to SE Asia, the regional structural orientations/patterns are fundamentally controlled by the regional tectonic settings. Thus, the deformation events/styles must reflect regional tectonic setting. Despite the diverse lithologies and different metamorphic condition, if East Asia had

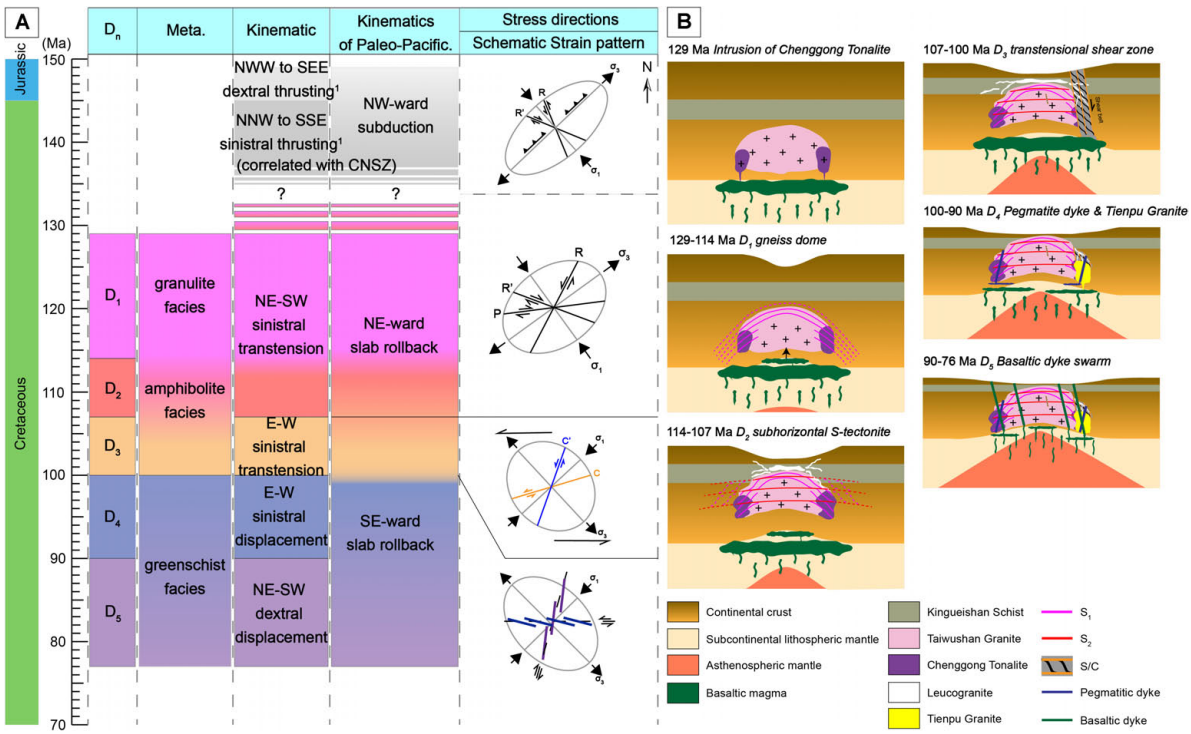

FIGURE 13 | A compiled diagram showing the structural and tectonic evolution of the Kinmen Island. **(A)** Composite diagram showing the reconstructed structural evolution and the associated plate kinematics and the schematic strain pattern. The structural evolution of Kinmen is correlated to the regional-scale Changle-Nanao Shear Zone (superscript 1; Shi, 2011). Besides, the normal fault systems of the extensional basins within the Cathaysia Block (Li J. et al., 2014) is compiled to constrain the stress field during D_1–D_2. **(B)** Schematic diagram of the tectonic evolution of the Kinmen Island between 129 and 76 Ma. Both horizontal and vertical dimensions are not to scale.

undergone extensive crustal thinning, extensional stress should be a more reasonable explanation for the development of these reported Early Cretaceous structures.

Correlation to the Stress Evolution of Cretaceous Extensional Basins Within SE Asia

Numerous early Cretaceous (145–100 Ma) NE-trending and WNW-ESE trending intracontinental extensional basins are bounded by high-angle normal faults within the Cathaysia Block (e.g., Shu et al., 2009; Li J. et al., 2014). The development of these sedimentary basins and their boundary normal fault systems reflected the stress setting during their formation. These boundary normal fault systems indicated general stress pattern of NW-SE extension around 136–118 Ma, and NW-SE transpression around 118–107 Ma. The extension direction switched to NWW-SEE during 107–85 Ma, WNW-ESE transpression around 85 Ma, and to N-S extension during 80–65 Ma. The schematic strain pattern derived from our reconstructed structural evolution reveals similar yet more detailed stress evolution along the coast of SE Asia (**Figure 13A**). From 150 to 137 Ma, the continental crust was under NW-SE compression (σ_1) with NE-SW extension (σ_3) due to the forward subduction of the Paleo-Pacific plate. The stress pattern switched to NE-SW extension (σ_3) with NW-SE compression (σ_1) during ~129–107 Ma (our D_1 and D_2) as the crust extended due to the northeastward rollback of the Paleo-Pacific plate. Owing to the changing rollback direction into southeastward, the stress setting shifted to NW-SE extension (σ_3) and NE-SW compression (σ_1) during 107–76 Ma (our D_3–D_5). Most of the previous studies interpreted the NE-striking mylonitic foliation as the main structure (S/C fabric) of the CNSZ (Tong and Tobisch, 1996; Wang and Lu, 2000; Chen et al., 2002; Wei et al., 2015). In this study, well-developed S/C/C' fabrics (**Figures 3**, **7A,F,H**, **13A**) are noted. The S/C/C' fabrics allow us to decipher the non-coaxial sinistral shearing setting under NW-SE extension (σ_3) and NE-SW compression (σ_1) stress pattern for the D_3 event (**Figure 13A**). Likewise, rather than WNW-ESE transpression and N-S extension, if we consider our D_4 pegmatites and D_5 basalt dykes to form along the shear fractures under the same stress setting as D_3, NW-SE extension with NE-SW compression is adequate to produce such structural pattern.

Changing Direction of the Paleo-Pacific Plate Rollback

According to our reconstructed structural evolution in the Kinmen Island, two stress fields of NW-SE compression (σ_1) with NE-SW extension (σ_3) for D_1 to D_2, and NE-SW compression (σ_1) with NW-SE extension (σ_3) from D_3 till D_5 are delineated. Our reconstructed stress field evolution could be linked to

the changing direction of slab rollback of the Paleo-Pacific plate as indicated by the maximum extension direction (σ_3). The northeastward slab rollback correlates nicely with the northeastward younging trend of the 180–125 Ma igneous rocks within the Cathaysia Block as Wang et al. (2011) proposed. The oblique subduction might have triggered the strike-slip deformation within the overriding plates (Holdsworth et al., 1998) while the slab rollback might have induced the back-arc extension of the continental lithosphere, as demonstrated by the geodynamic modeling (Chen et al., 2016). It's suggested that the northeastward slab rollback satisfies the oblique divergence setting and could have initiated the sinistral shear zone (e.g., CNSZ) and numerous NE-SW and WNW-ESE normal fault systems (**Figure 13A**). In light of the 149–137 Ma NW-SE thrusting of CNSZ (Shi, 2011), we prefer a northwestward forward subduction of the Paleo-Pacific plate during this period but not southwestward oblique subduction. Accordingly, the crustal extension along the coast of SE Asia was initiated during 137–129 Ma, consistent with the previous studies of 135–90 Ma crustal extension (Dong et al., 2018). The stress field changed to NE-SW compression (σ_1) with NW-SE extension (σ_3) during 114–107 Ma as the direction of slab rollback shifted to southeastward when the Cathaysia Block is characterized by the magmatic quiescence (118–107 Ma, Li J. et al., 2014). The alternation of σ_1 and σ_3 between $D_{1\sim2}$ then to $D_{3\sim5}$ demonstrates that all observed structures of this study are mainly developed or reactivated along two weak zones that reflect the slab rollback direction.

Tectonic and Crustal Evolution of the Kinmen Island

During early Cretaceous time, numerous granitoid batholiths intruded along the coast of SE Asia, including PDMB (Li et al., 2015) and the Kinmen Island (e.g., Taiwushan Granite and Chenggong Tonalite). The northeastward rollback of the Paleo-Pacific plate initiated the continental crust extension and post-orogenic magmatism (e.g., Taiwushan Granite in Kinmen; Lan et al., 1997). This NE-ward slab rollback imposed the NE-SW extension on the crust, which generated the kilometer-scale gneiss dome (D_1; 129–114 Ma) in the Kinmen Island and NE-SW extensional folding within the PDMB. The slab-rollback-induced extension thinned the continental crust by opening of the extensional basins, denudation of the upper brittle crust and exhumation of ductile lower-to-middle crust. The crustal thinning resulted from the bulk extension triggered the middle to lower crustal flow (Teyssier and Whitney, 2002) along with the exhumation of the gneiss dome to form the subhorizontal S-tectonite (D_2; 114–107 Ma). The further crustal thinning and vertical displacement of the gneiss dome due to the sustained slab rollback and the density-inversion diapiric flow triggered the ENE-WSW striking sinistral transtensional shear zone (D_3; 107–100 Ma). The exhumation of the gneiss dome into the middle crust during D_2–D_3 produced the longstanding magmatism of leucogranite from pre-D_2 to post-D_3 and related amphibolite facies metamorphism owing to the decompression melting. Under the same stress setting of southeastward slab rollback as D_3, the continental crust was continually uplifted into upper crust in D_4 (100–90 Ma) with intrusion of Tienpu Granite and later pegmatites along E-W striking extensional shear fractures marking the end of ductile deformation. The final D_5 (90–76 Ma) was NE-SW striking mafic dike swarms sourced from the upwelling asthenosphere, representing the almost rifting stage of continental crust (**Figure 13B**).

CONCLUSION

The granitic batholiths within the Kinmen Island record the crustal thinning history of the southeast coast of China during the Cretaceous period, induced by the longstanding slab rollback of the Paleo-Pacific plate from 139 to 76 Ma. Based on our reconstructed structural evolution and petrographic analysis, five deformation events accompanied with the exhumation of deep-seated granitoids and the associated stress field was revealed. The kilometer-scale gneiss dome (D_1; 129∼114 Ma) was formed at lower continental crust under granulite facies condition post the intrusion of the Chenggong Tonalite (G_1). Further crustal thinning and exhumation of the gneiss dome generated subhorizontal S-tectonite (D_2; 114∼107 Ma) under upper amphibolite facies. The stress field of D_1 and D_2 was both under NW-SE compression with NE-SW extension due to the northeastward slab rollback of the Paleo-Pacific plate. The local development of ENE-WSW striking sinistral transtensional shear zones under amphibolite facies condition (D_3; 107∼100 Ma) were initiated under NW-SE extension as the slab rollback direction of Paleo-Pacific plate shifted to southeast. This strongly developed transtensional shear zones facilitated not only the exhumation of the gneiss dome to the upper continental crust, but also decompressional melting to form the G_2 leucogranite. With further slab rollback and the crustal thinning, the 100 Ma Tienpu Granite (G_3) intruded both the Chenggong Tonalite (G_1) and the leucogranite (G_2) on account of decompression melting of the upwelling asthenosphere. Under the same stress setting of NW-SE extension, the E-W striking pegmatitic dykes (D_4/G_4; 100∼90 Ma) were emplaced, and were followed by the intrusion of NE-SW striking mafic dike swarms (D_5/G_5; 90∼76 Ma) as the continental crust was almost rifted as a consequence of the prolonged crustal extension caused by continual slab rollback of the Paleo-Pacific plate.

DATA AVAILABILITY STATEMENT

All datasets presented in this study are included in the article/**Supplementary Material**.

AUTHOR CONTRIBUTIONS

Both authors contributed to the design, field, sample collection, conception of this study, the interpretation of data, manuscript writing, revision, and read and approved the submitted version. T-HH was responsible to the data compilation and thin section making and petrography analysis.

FUNDING

This research received funding support from the Ministry of Science and Technology of Taiwan under project ID: 105WFA0350331 and 107-2813-C-002-113-M. The funding supports the field work and analytical instruments.

ACKNOWLEDGMENTS

Dr. M. F. Chu is thanked for her input on the discussion about the igneous petrogenesis in our study area. Besides, we appreciate the aerial photos provided by Mr. C. H. Tsao to clearly identify the crosscutting relationships between the different lithologies. The Kinmen Weather Station is thanked for providing the accommodation. Finally, MOST of Taiwan is appreciated for their funding support under project IDs: 105WFA0350331 and 107-2813-C-002-113-M.

SUPPLEMENTARY MATERIAL

The Supplementary Material for this article can be found online at: https://www.frontiersin.org/articles/10.3389/feart.2020.00330/full#supplementary-material

TABLE S1 | Measured structural data in the form of dip direction and dip for planar structures, and as trend and plunge for linear structures.

REFERENCES

Berger, A., and Stünitz, H. (1996). Deformation mechanisms and reaction of hornblende: examples from the Bergell tonalite (Central Alps). *Tectonophysics* 257, 149–174. doi: 10.1016/0040-1951(95)00125-5

Blythe, A. E. (1998). "Active tectonics and ultrahigh-pressure rocks," in *When Continents Collide: Geodynamics and Geochemistry of Ultrahigh-Pressure Rocks*, eds B. Hacker and J.G. Liou (Dordrecht: Springer), 141–160. doi: 10.1007/978-94-015-9050-1_6

Chen, C. H., Lin, W., Lan, C. Y., and Lee, C. Y. (2004). Geochemical, Sr and Nd isotopic characteristics and tectonic implications for three stages of igneous rock in the Late Yanshanian (Cretaceous) orogeny, SE China. *Earth Environ. Sci. Trans. R. Soc. Edinburgh* 95, 237–248. doi: 10.1017/s0263593300001048

Chen, W. S., Yang, H. C., Wang, X., and Huang, H. (2002). Tectonic setting and exhumation history of the Pingtan–Dongshan metamorphic belt along the coastal area, Fujian Province, Southeast China. *J. Asian Earth Sci.* 20, 829–840. doi: 10.1016/s1367-9120(01)00066-9

Chen, Z., Schellart, W. P., Strak, V., and Duarte, J. C. (2016). Does subduction-induced mantle flow drive backarc extension? *Earth Planet. Sci. Lett.* 441, 200–210. doi: 10.1016/j.epsl.2016.02.027

Chiu, Y. P., Yeh, M. W., Wu, K. H., Lee, T. Y., Lo, C. H., Chung, S. L., et al. (2018). Transition from extrusion to flow tectonism around the Eastern Himalaya syntaxis. *GSA Bull.* 130, 1675–1696. doi: 10.1130/b31811.1

Dong, S., Zhang, Y., Li, H., Shi, W., Xue, H., Li, J., et al. (2018). The Yanshan orogeny and late Mesozoic multi-plate convergence in East Asia—Commemorating 90th years of the "Yanshan Orogeny". *Sci. China Earth Sci.* 61, 1888–1909. doi: 10.1007/s11430-017-9297-y

Döpke, D. (2017). *Modelling the Thermal History of Onshore Ireland, Britain and Its Offshore Basins Using Low-temperature Thermochronology*. Doctoral dissertation, Trinity College Dublin, Ireland.

Gleadow, A. J. W., and Duddy, I. R. (1981). A natural long-term track annealing experiment for apatite. *Nuclear Tracks* 5, 169–174. doi: 10.1016/0191-278x(81)90039-1

Harrison, T. M. (1982). Diffusion of 40Ar in hornblende. *Contrib. Mineral. Petrol.* 78, 324–331. doi: 10.1007/bf00398927

Harrison, T. M., and McDougall, I. (1982). The thermal significance of potassium feldspar K-Ar ages inferred from 40Ar39Ar age spectrum results. *Geochim. Cosmochim. Acta* 46, 1811–1820. doi: 10.1016/0016-7037(82)90120-x

Holdsworth, R. E., Strachan, R. A., and Dewey, J. F. (eds) (1998). *Continental Transpressional and Transtensional Tectonics*. London: Geological Society.

Hsü, K. J., Li, J., Chen, H., Wang, Q., Sun, S., and Şengör, A. M. C. (1990). Tectonics of South China: key to understanding West Pacific geology. *Tectonophysics* 183, 9–39. doi: 10.1016/0040-1951(90)90186-c

Huang, L., Wang, L., Fan, H. R., Lin, M., and Zhang, W. (2019). Late early-cretaceous magma mixing in the langqi island, fujian province, china: evidences from petrology, geochemistry and zircon geochronology. *J. Earth Sci.* 31, 468–480. doi: 10.1007/s12583-019-1022-7

John, B. M., Zhou, X. H., and Li, J. L. (1990). Formation and tectonic evolution of southeastern China and Taiwan: isotopic and geochemical constraints. *Tectonophysics* 183, 145–160. doi: 10.1016/0040-1951(90)90413-3

Lan, C. Y., Chung, S. L., and Mertzman, S. A. (1997). Mineralogy and geochemistry of granitic rocks from Chinmen, Liehyu and Dadan Islands, Fujian. *J. Geol. Soc. China* 40, 527–558.

Lan, C. Y., Chung, S. L., Mertzman, S. A., and Chen, C. H. (1995). Mafic dykes from Chinmen and Liehyu Islands, off Southeast China: petrochemical characteristics and tectonic implications. *J. Geol. Soc. China* 38, 183–213.

Lee, C. Y. (1994). *Chronology and Geochemistry of Basaltic Rocks from Penghu Islands and Mafic Dykes from East Fujian: Implications for The Mantle Evolution of SE China Since Late Mesozoic*. Doctoral dissertation, National Taiwan University, Taipei.

Lee, J. K., Williams, I. S., and Ellis, D. J. (1997). Pb, U and Th diffusion in natural zircon. *Nature* 390, 159–162. doi: 10.1038/36554

Li, J., Zhang, Y., Dong, S., and Johnston, S. T. (2014). Cretaceous tectonic evolution of South China: a preliminary synthesis. *Earth Sci. Rev.* 134, 98–136. doi: 10.1016/j.earscirev.2014.03.008

Li, X. H. (2000). Cretaceous magmatism and lithospheric extension in Southeast China. *J. Asian Earth Sci.* 18, 293–305. doi: 10.1016/s1367-9120(99)00060-7

Li, Y., Ma, C. Q., Xing, G. F., and Zhou, H. W. (2015). The early cretaceous evolution of SE China: insights from the changle–nan'ao metamorphic belt. *Lithos* 230, 94–104. doi: 10.1016/j.lithos.2015.05.014

Li, Z., Qiu, J. S., and Yang, X. M. (2014). A review of the geochronology and geochemistry of Late Yanshanian (Cretaceous) plutons along the Fujian coastal area of southeastern China: implications for magma evolution related to slab break-off and rollback in the Cretaceous. *Earth Sci. Rev.* 128, 232–248. doi: 10.1016/j.earscirev.2013.09.007

Li, Z., Zhou, J., Mao, J., Santosh, M., Yu, M., Li, Y., et al. (2013). Zircon U–Pb geochronology and geochemistry of two episodes of granitoids from the northwestern Zhejiang Province, SE China: implication for magmatic evolution and tectonic transition. *Lithos* 179, 334–352. doi: 10.1016/j.lithos.2013.07.014

Li, Z. X., and Li, X. H. (2007). Formation of the 1300-km-wide intracontinental orogen and postorogenic magmatic province in Mesozoic South China: a flat-slab subduction model. *Geology* 35, 179–182.

Lin, W. (1994). *Geochemistry and Thermal History of Late Yanshanian Granites from Chinmen Area*. Master thesis, National Taiwan University, Taipei.

Lin, W., Lee, C. Y., Yang, H. C., and Chen, C. H. (2011). *Geological Map of Taiwan scale 1:50000, Kinmen Area*. Kolkata: Central Geological Survey.

Liu, L., Xu, X., and Xia, Y. (2016). Asynchronizing paleo-Pacific slab rollback beneath SE China: insights from the episodic Late Mesozoic volcanism. *Gondwana Res.* 37, 397–407. doi: 10.1016/j.gr.2015.09.009

Liu, Q., Yu, J. H., Wang, Q., Su, B., Zhou, M. F., Xu, H., et al. (2012). Ages and geochemistry of granites in the Pingtan–Dongshan Metamorphic Belt, Coastal South China: new constraints on Late Mesozoic magmatic evolution. *Lithos* 150, 268–286. doi: 10.1016/j.lithos.2012.06.031

Lo, L. C. H., Onstott, T. C., and Lee, W. L. C. W. (1993). 40Ar/39Ar dating of plutonic/metamorphic rocks from Chinmen Island off Southeast China and its tectonic implications. *J. Geol. Soc. China* 36, 35–55.

Mai, H. A., Chan, Y. L., Yeh, M. W., and Lee, T. Y. (2018). Tectonic implications of Mesozoic magmatism to initiation of Cenozoic basin development within

the passive South China Sea margin. *Int. J. Earth Sci.* 107, 1153–1174. doi: 10.1007/s00531-017-1537-y

Mao, J., Li, Z., and Ye, H. (2014). Mesozoic tectono-magmatic activities in South China: retrospect and prospect. *Sci. China Earth Sci.* 57, 2853–2877. doi: 10.1007/s11430-014-5006-1

McDougall, I., and Harrison, T. M. (1999). *Geochronology and Thermochronology by the 40Ar/39Ar Method*. Oxford: Oxford University Press.

Sheldrick, T. C., Barry, T. L., Dash, B., Gan, C., Millar, I. L., Barfod, D. N., et al. (2020). Simultaneous and extensive removal of the East Asian lithospheric root. *Sci. Rep.* 10, 1–6.

Shi, J. J. (2011). Dividing of deformation and metamorphic stages and determination of its ages in Changle-Nanao tectonic zone. *Geol. Fujian* 3, 189–199.

Shu, L. S., Zhou, X. M., Deng, P., Wang, B., Jiang, S. Y., Yu, J. H., et al. (2009). Mesozoic tectonic evolution of the Southeast China Block: new insights from basin analysis. *J. Asian Earth Sci.* 34, 376–391. doi: 10.1016/j.jseaes.2008.06.004

Stipp, M., StuÈnitz, H., Heilbronner, R., and Schmid, S. M. (2002). The eastern Tonale fault zone: a 'natural laboratory'for crystal plastic deformation of quartz over a temperature range from 250 to 700 C. *J. Struct. Geol.* 24, 1861–1884. doi: 10.1016/s0191-8141(02)00035-4

Sun, W., Ding, X., Hu, Y. H., and Li, X. H. (2007). The golden transformation of the Cretaceous plate subduction in the west Pacific. *Earth Planet. Sci. Lett.* 262, 533–542. doi: 10.1016/j.epsl.2007.08.021

Teyssier, C., and Whitney, D. L. (2002). Gneiss domes and orogeny. *Geology* 30, 1139–1142.

Tong, W. X., and Tobisch, O. T. (1996). Deformation of granitoid plutons in the Dongshan area, southeast China: constraints on the physical conditions and timing of movement along the Changle-Nanao shear zone. *Tectonophysics* 267, 303–316. doi: 10.1016/s0040-1951(96)00107-2

Wang, F. Y., Ling, M. X., Ding, X., Hu, Y. H., Zhou, J. B., Yang, X. Y., et al. (2011). Mesozoic large magmatic events and mineralization in SE China: oblique subduction of the Pacific plate. *Int. Geol. Rev.* 53, 704–726. doi: 10.1080/00206814.2010.503736

Wang, Y., Fan, W., Zhang, G., and Zhang, Y. (2013). Phanerozoic tectonics of the South China Block: key observations and controversies. *Gondwana Res.* 23, 1273–1305. doi: 10.1016/j.gr.2012.02.019

Wang, Z. H., and Lu, H. F. (2000). Ductile deformation and 40Ar/39Ar dating of the Changle–Nanao ductile shear zone, southeastern China. *J. Struct. Geol.* 22, 561–570. doi: 10.1016/s0191-8141(99)00179-0

Wei, W., Faure, M., Chen, Y., Ji, W., Lin, W., Wang, Q., et al. (2015). Back-thrusting response of continental collision: early cretaceous NW-directed thrusting in the Changle-Nan'ao belt (Southeast China). *J. Asian Earth Sci.* 100, 98–114. doi: 10.1016/j.jseaes.2015.01.005

Wong, J., Sun, M., Xing, G., Li, X. H., Zhao, G., Wong, K., et al. (2009). Geochemical and zircon U–Pb and Hf isotopic study of the Baijuhuajian metaluminous A-type granite: extension at 125–100 Ma and its tectonic significance for South China. *Lithos* 112, 289–305. doi: 10.1016/j.lithos.2009.03.009

Xie, G. Q., Hu, R. Z., Zhao, J. H., and Jiang, G. H. (2001). Mantle plume and the relationship between it and Mesozoic large-scale metallogenesis in southeastern China: a preliminary discussion. *Geotectonica Metallogenia* 25, 179–186.

Yang, J., Zhao, Z., Hou, Q., Niu, Y., Mo, X., Sheng, D., et al. (2018). Petrogenesis of Cretaceous (133–84 Ma) intermediate dykes and host granites in southeastern China: implications for lithospheric extension, continental crustal growth, and geodynamics of Palaeo-Pacific subduction. *Lithos* 296, 195–211. doi: 10.1016/j.lithos.2017.10.022

Yang, S. Y., Jiang, S. Y., Zhao, K. D., Jiang, Y. H., Ling, H. F., and Luo, L. (2012). Geochronology, geochemistry and tectonic significance of two Early Cretaceous A-type granites in the Gan-Hang Belt, Southeast China. *Lithos* 150, 155–170. doi: 10.1016/j.lithos.2012.01.028

Yui, T. F., Heaman, L., and Lan, C. Y. (1996). U-Pb and Sr isotopic studies on granitoids from Taiwan and Chinmen-Lieyu and tectonic implications. *Tectonophysics* 263, 61–76. doi: 10.1016/s0040-1951(96)00023-6

Zhang, Y. Q., Dong, S. W., Li, J. H., Cui, J. J., Shi, W., Su, J. B., et al. (2012). The new progress in the study of Mesozoic tectonics of South China. *Diqiu Xuebao* 33, 257–279.

Zhao, J. H., Hu, R., Zhou, M. F., and Liu, S. (2007). Elemental and Sr–Nd–Pb isotopic geochemistry of Mesozoic mafic intrusions in southern Fujian Province, SE China: implications for lithospheric mantle evolution. *Geol. Magaz.* 144, 937–952. doi: 10.1017/s0016756807003834

Zhao, X., Jiang, Y., Xing, G., Chen, Z., Liu, K., Yu, M., et al. (2018). A geochemical and geochronological study of the Early Cretaceous, extension-related Honggong ferroan (A-type) granite in southwestern Zhejiang Province, southeast China. *Geol. Magaz.* 155, 549–567. doi: 10.1017/s0016756816000790

Zhou, B. X., Sun, T., Shen, W., Shu, L., and Niu, Y. (2006). Petrogenesis of Mesozoic granitoids and volcanic rocks in South China: a response to tectonic evolution. *Episodes* 29:26. doi: 10.18814/epiiugs/2006/v29i1/004

Zhou, X. M., and Li, W. X. (2000). Origin of Late Mesozoic igneous rocks in Southeastern China: implications for lithosphere subduction and underplating of mafic magmas. *Tectonophysics* 326, 269–287. doi: 10.1016/s0040-1951(00)00120-7

Conflict of Interest: The authors declare that the research was conducted in the absence of any commercial or financial relationships that could be construed as a potential conflict of interest.